S.T. Yau High School Science Award

Research Report

The Team
Name of team member: Andrew Liu
School: Thacher School
City, Country: Ojai, United States

Name of supervising teacher: Tyler Ortiz
Job Title: Mathematics Teacher
School/Institution: Thacher School
City, Country: Ojai, United States

Title of Research Report
RescuePulse: A Bio-inspired Robot Leveraging Self-Excited Oscillation and Physical Intelligence for Post-Disaster Confined-Space Search

Date
09/12/2026

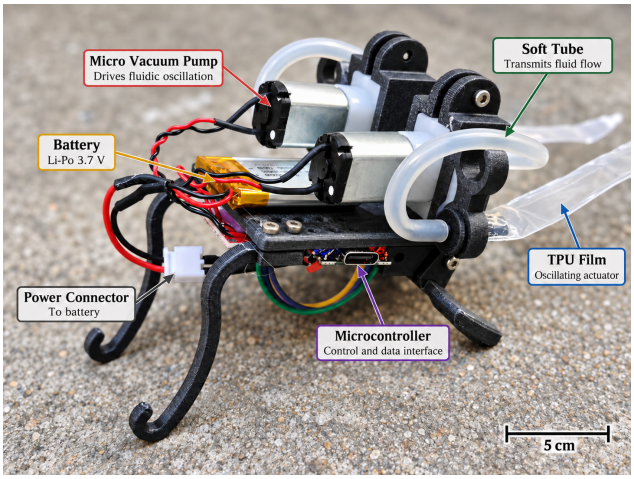
Abstract

In post-disaster environments, there often exist many narrow, unstable and difficult-to-access spaces or channels. This not only significantly increases the risk for rescue personnel to directly enter, but also hinders the rapid arrival of life detection, environmental perception and disaster assessment at the target area, thereby delaying the location of trapped individuals and the formulation of rescue decisions. The existing robot platforms, including wheeled or tracked inspection robots, snake-like robots, and pneumatic soft robots, although have improved accessibility in confined environments, still face some significant limitations. For instance, their movement capabilities on slippery surfaces are insufficient, and their mechanical structures or control systems are relatively complex. These issues restrict the reliability and environmental adaptability of robots in post-disaster search, inspection, and rescue tasks in confined spaces.

To address these challenges, this study proposes a new generation of confined-space search robots, RescuePulse, inspired by insect movement and based on self-excited oscillation(See Graphical Abstract). The robot employs two circumferentially distributed self-excited oscillation units, each driven by an independent micro air pump. The two units generate continuous rhythmic motion without requiring complex electronic timing control. By adjusting the flow rates on both sides, the system can achieve smooth linear advancement and also complete active steering through differential output forces.

Firstly, the parameters of the robot were optimized. As the airflow flow rate increased and the fluid channel size decreased, the self-excited oscillation frequency showed an overall upward trend. The optimal oscillation unit size determined through experiments was 10 mm × 80 mm. At a flow rate of 0.8 L/min, the oscillation frequency was approximately 5.2 Hz. Secondly, this project studied the movement ability of the self-excited oscillation robot in narrow and humid environments. The experiments showed that in a narrow environment, the robot achieved an average forward speed of 0.418 mm/s and an average angular velocity of 2.33°/s, and successfully moved through 80-120 mm pipes even under humid conditions. Finally, comparative tests showed that **the robot moved 2.2 times faster than a traditional airbag-type robot in a straight pipe and achieved a 100% success rate in a 150° bend, compared with 40% success rate for the airbag-type robot.**

These results indicate that integrating the self-excited oscillation mechanism with physical intelligence enables **RescuePulse robot** to achieve continuous axial propulsion and active steering without the need for complex electronic or mechanical control systems. **More importantly, this approach is expected to enhance the robot's ability to pass through and adapt to restricted spaces in post-disaster situations, such as narrow, curved, damp, and irregularly structured areas.** This study focuses on validating self-excited oscillation as a feasible locomotion mechanism for post-disaster confined-space robots. Future work will investigate the integration of perception payloads, such as cameras and environmental or life-detection sensors. The RescuePulse will support safer remote inspection and search-and-rescue operations while reducing rescuers' direct exposure to danger.



Graphical Abstract: The bio-inspired soft robot uses self-excited fluidic oscillation to generate rhythmic locomotion and differential steering for post-disaster confined-space exploration.

Keywords: Self-excited Oscillation, Bio-inspired Robot, Pneumatic Actuation

Commitments on Academic Honesty and Integrity

We hereby declare that we

1. are fully committed to the principle of honesty, integrity, and fair play throughout the competition.
2. actually perform the research work ourselves and thus truly understand the content of the work.
3. observe the common standard of academic integrity adopted by most journals and degree theses.
4. have declared all the assistance and contribution we have received from any personnel, agency, institution, etc. for the research work.
5. undertake to avoid getting in touch with assessment panel members in a way that may lead to direct or indirect conflict of interest.
6. undertake to avoid any interaction with assessment panel members that would undermine the neutrality of the panel member and fairness of the assessment process.
7. observe the safety regulations of the laboratory(ies) where we conduct the experiment(s), if applicable.
8. observe all rules and regulations of the competition.
9. agree that the decision of YHSA is final in all matters related to the competition.

We understand and agree that failure to honour the above commitments may lead to disqualification from the competition and/or removal of reward, if applicable; that any unethical deeds, if found, will be disclosed to the school principal of team member(s) and relevant parties if deemed necessary; and that the decision of YHSA is final and no appeal will be accepted.

(Signatures of full team below)



Name of team member: Andrew Liu



Name of supervising teacher: Tyler Ortiz

Contents

1 Introduction **1**
- 1.1 Background . . . 1
- 1.2 Existing Works . . . 1
- 1.3 Research Innovations . . . 2

2 Bio-Inspired Locomotion via Physical Self-Excited Oscillation **3**
- 2.1 The mechanism of insect's movement . . . 3
- 2.2 From Air Dancers to Insect-Like Rhythmic Locomotion . . . 4
- 2.3 The physical principle of self-excited oscillation . . . 5
  - 2.3.1 Self-excited oscillation mechanism of flat ring tube . . . 5
  - 2.3.2 Factors that affect oscillation characteristics . . . 6
  - 2.3.3 Mechanical properties and self-excited oscillation of inflatable structures . . . 7
- 2.4 Chapter Summary . . . 8

3 Design and Implementation of the Self-Excited Oscillation Unit **8**
- 3.1 Material Selection and Environmental Adaptability . . . 8
- 3.2 Design of Self-Excited Unit Structure . . . 11
- 3.3 Design and Fabrication of TPU Tubes . . . 11
- 3.4 Performance Experiment of Self-Excited Oscillation Unit . . . 13
  - 3.4.1 Experimental Objectives and Design . . . 13
  - 3.4.2 Frequency Extraction Method . . . 13
  - 3.4.3 Results and Analysis . . . 14
  - 3.4.4 Determination of Unit Size . . . 16
- 3.5 Chapter Summary . . . 16

4 Robot System Integration and Confined-Space Adaptation **17**
- 4.1 Overall Mechanical Integration of the Robot . . . 17
  - 4.1.1 Mechanical Structure Design . . . 17
  - 4.1.2 Gait Generation Mechanism . . . 19
- 4.2 Experimental Verification of Motion Performance . . . 20
  - 4.2.1 Axial thrust capability test experiment . . . 20
  - 4.2.2 Steering Ability Test Experiment . . . 21
- 4.3 Environmental Adaptability Experiment . . . 23
  - 4.3.1 Motion Performance in Confined Passages of Different Diameters . . . 23
- 4.4 Chapter Summary . . . 25

5 Comparative Experiments and Post-Disaster Environment Validation **25**
- 5.1 Design and Fabrication of the Airbag Robot . . . 26
- 5.2 Comparative Experiment of Axial Motion Capabilities of Airbag Robot and Self-Excited Oscillating Robot in Straight Pipeline . . . 27
- 5.3 Comparative Experiment in a Curved Pipe . . . 29
- 5.4 Adaptability Experiment in a Simulated Rubble Environment . . . 31
  - 5.4.1 Curved-Path Locomotion in the Rubble Environment . . . 31
  - 5.4.2 Passage Through a Narrow Rubble Gap . . . 31
- 5.5 Comprehensive Analysis . . . 32
- 5.6 Chapter Summary . . . 33

6 Conclusions and Outlook **33**
- 6.1 Summary of Research Work . . . 33
- 6.2 Outlook . . . 34

Reference **34**

Appendix I **35**

Acknowledgments **37**

1 Introduction

1.1 Background

The earthquakes, building collapses and underground space accidents in recent years have demonstrated that the rapid exploration of narrow and confined spaces in disaster-stricken areas is a crucial aspect in search and rescue operations. The 2023 Turkey-Syria earthquake in Turkey caused extensive overall or partial collapses of buildings, and rescue personnel had to continuously search for survivors in the complex ruins composed of concrete, steel bars and building debris. As time passed, factors such as low temperatures, structural damage and difficult access to internal spaces further reduced the possibility of successful rescue [1]. The 2025 Myanmar earthquake also caused extensive building damage. After a building collapsed in Bangkok, rescue personnel had to search for dozens of possible trapped individuals in a large amount of debris and constrained space, further highlighting the importance of rapid detection of collapsed structure internal spaces [2]. Apart from building collapses, underground confined space accidents also present similar challenges. For example, in the 2023 tunnel collapse accident in the northern state of Uttarakhand, India, 41 workers were trapped underground for 17 days. Eventually, they were rescued by continuous drilling and the creation of rescue channels [3]. **These events illustrate that the trapped individuals are often located in deep spaces with narrow entrances, curved paths, unstable structures and inaccessible exteriors.** Rescue personnel and conventional equipment have difficulty entering these areas promptly and safely, thereby increasing the difficulty of personnel positioning, internal environment judgment and rescue route planning.

The "reachability" aspect has long been regarded as a core technical bottleneck in the field of urban search and rescue. The National Institute of Standards and Technology (NIST) pointed out that Urban Search and Rescue is a highly dangerous and time-sensitive task. Robots can reduce the risk of rescue personnel being directly exposed to dangerous areas by entering collapsed structures, searching for trapped individuals, identifying potential hazards, and establishing internal environmental information [4]. NIST's description of typical post-disaster subsurface voids further indicates that these spaces often have narrow entrances, continuous bends, complex supporting surfaces, low visibility, dampness, and potential hazardous substances, and even traditional search cameras may be unable to reach the target area due to being unable to bypass corners [5]. Therefore, the key to exploring narrow spaces after disasters is not only about "what can be perceived", but also about how to reliably send cameras, audio, and environmental sensing equipment into deep and restricted spaces that humans cannot safely enter. **Miniaturized and flexible robots with active steering and strong passage capability in complex confined environments have the potential to serve as pre-sensing platforms for rescue teams, providing critical information for life-sign detection, hazardous-environment assessment, and subsequent rescue planning and decision-making.**

1.2 Existing Works

Currently, robots used for search and inspection in confined spaces after disasters mainly include wheeled and tracked robots, snake-like, and pneumatic soft robots. Wheeled and tracked platforms feature mature mobility mechanisms and strong load-bearing capacity, enabling them to carry cameras, environmental sensors, and communication equipment, and have thus been deployed in real disaster scenarios for building inspection and search missions. Surmann et al. summarized multiple actual deployments of the German Rescue Robotics Center in damaged buildings, demonstrating the ability of wheeled and tracked robots to conduct remote exploration in ruins, staircases, and interior of dangerous buildings. At the same time, they also pointed out that complex terrain, loose surfaces, and communication conditions would limit the continuous movement and remote operation of the robots [6]. Recent reviews on search and rescue robots have also pointed out that in environments where Global Navigation Satellite System(GNSS) signals are absent, such as underground, caves, and disaster areas, complex terrain, low visibility, structural dynamic changes, and narrow and crowded spaces significantly increase the difficulty of wheeled and tracked robot positioning, autonomous exploration, and reliable operation [7].

In contrast, the snake-shaped robot relies on its slender body and multiple connected joints to be able to enter the narrow cracks in ruins that traditional wheeled and tracked robots find difficult to access. Jadeja et al. proposed a snake-shaped robot for search and rescue of survivors after earthquakes in 2024. They integrated visual perception at the front end of the robot and compared deep learning algorithms such as

Faster R-CNN, SSD, and YOLO for identifying trapped individuals, demonstrating the potential of the snake-shaped robot as a platform for sensing deep spaces in post-disaster situations [8]. However, such robots usually require multiple connected joints, actuators, and coordinated gait and posture control. Their high degree of freedom structure not only enhances maneuverability but also increases the complexity of mechanical structures, motion planning, and control systems.

Another important type of solution are soft and worm-like pneumatic robots. These robots typically achieve unicycle propulsion through radial expansion, axial elongation, and periodic anchoring-release processes. The soft structure can conform to the geometries of pipes and narrow passages. Blewitt et al. conducted a systematic review in 2024 on worm-like pipeline inspection robots, stating that these robots form a wriggling gait through radial expansion and axial elongation and have good morphological adaptability for small pipes and confined spaces [9]. However, this review also pointed out that, for real-world applications, complex pipe networks require further research on steering, path selection, actuator coordination, sensor integration, and reliable control; many pneumatic schemes still require multiple actuators and the corresponding inflation-disinflation control processes to form periodic movements.

Based on the above analysis, this project compared the robot solutions for existing confined spaces (see Table 1-1). In summary, the existing robots in confined spaces exhibit a common technical trade-off: **greater environmental adaptability often relies on more mechanical degrees of freedom, the number of actuators, or more complex control strategies.** Wheeled/track robots have a relatively mature engineering platform, but their maneuverability is still limited in extremely irregular and constrained environments; snake robots achieve good turning ability by increasing joint degrees of freedom, but this comes with higher mechanical and control complexity; traditional pneumatic soft robots have good flexibility, but often require multiple pneumatic actuators and periodic control sequences. Therefore, how to maintain the robot's flexibility and the ability to pass through complex channels while reducing the complexity of basic motion control and achieving stable active steering remains an important issue in the research of robots in post-disaster confined spaces. **There is a need to develop the next-generation robots that can effectively adapt to confined environments while simultaneously achieving low-complexity motion control and high mobility.**

Table 1-1: Summary and Comparison of Existing Confined-Space Robotic Systems

Type	**Representative Work**	**Main Limitations**	**Advantages of RescuePulse**
Wheeled/Tracked Robots	Surmann et al. [6]	Motion and communication remain limited in loose, irregular terrain and complex building environments.	Compliant structure improves adaptability to narrow, curved, and humid spaces.
Snake-like Robots	Jadeja et al. [8]	Multiple joints and actuators lead to relatively high mechanical and control complexity.	Dual-unit design reduces mechanical and control complexity.
Pneumatic Worm-like Robots	Blewitt et al. [9]	Multiple actuators and timing-control sequences are often required; complex steering and navigation in real environments remain challenging.	Self-excited oscillation enables rhythmic locomotion and differential steering without electronic timing control.

1.3 Research Innovations

This study develops RescuePulse, a self-excited oscillation robot for post-disaster confined-space locomotion. Its main contributions are summarized as follows:

1. **Reduced actuation complexity.** Existing snake-like and pneumatic robots often rely on multiple joints, actuators, or externally timed inflation–deflation sequences. RescuePulse instead generates periodic motion through self-excited fluid–structure interaction, reducing the need for complex gait-generation mechanisms.

2. **Simplified active steering.** Many confined-space robots achieve turning through multi-joint coordination or multiple independently controlled actuators. RescuePulse uses two symmetrically arranged oscillation units and differential airflow to generate steering torque, enabling both forward locomotion and directional control with a simpler mechanical architecture.

3. **Validation in confined and humid environments.** Existing robotic platforms often face reduced mobility in narrow, curved, or wet spaces. This study experimentally verifies that the proposed locomotion mechanism can operate in 80–120 mm confined passages, while maintaining forward motion and active steering under humid conditions.

The main objective of this study is therefore not to develop a complete sensing-and-rescue system, but to validate self-excited oscillation as a feasible locomotion principle for post-disaster confined-space robots. Future work will investigate the integration of cameras, environmental sensors, and life-detection payloads.

2 Bio-Inspired Locomotion via Physical Self-Excited Oscillation

2.1 The mechanism of insect's movement

When designing next-generation robots for exploration in confined spaces, the organisms that can move efficiently in narrow and irregular environments may provide us with creative bio-inspired inspiration. **What type of organism is the most representative? Yes, it's insects.** They can pass through narrow gaps, cross uneven surfaces, and constantly adjust their body posture during continuous movement, thus maintaining stable mobility.

Periodic reciprocating motion is the fundamental form of biological locomotion, which is particularly made evident in the swimming motion of fish and the crawling maneuver of insects. Dickinson et al. [10] demonstrate in their studies that the animal's locomotion operates not in a simple linear cascade but in a complex system formed by the dynamic coupling of the musculoskeletal, nervous, and environmental systems.

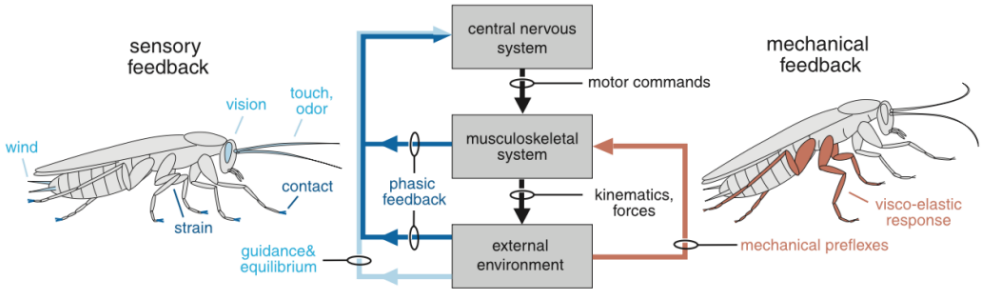


Figure 2-1: Model for locomotor control with sensory and mechanical feedback loops. [10]

Shown in Figure 2-1, the motion control model of a cockroach highlights two crucial feedback paths: sensory and mechanical feedback [10]. Central Pattern Generators (CPGs) are neural circuits in the nervous system that generate rhythmic oscillatory signals without sensory feedback, thereby driving limb muscles to produce periodic contractions [10]. CPGs serve as the neural basis for generating a stable gait for animals. Nevertheless, CPGs' output is not static, as the mechanical receptors distributed in tendons, muscles, and the body surface continuously monitor the position, speed, and force exerted by the limbs. The output of CPGs is also adjusted through rapid-phase feedback, allowing the movement pattern to adapt to environmental changes [10].

Interestingly, the viscoelastic properties of the musculoskeletal system itself provide a feedback mechanism that is faster than neural reflexes. Dickinson et al. described this mechanism, "preflex," in which the mechanical system is disturbed, allowing resistance to the disturbance through a passive elastic restoring force before the neural signal intervenes. Combining with neural reflexes and feedforward control, this mechanical feedback constitutes a robust control system for biological motion [10].

This biological mechanism provides significant inspiration for the design of robots operating in confined spaces, as it reveals how organisms coordinate their body mechanics with environmental interactions to move within narrow and irregular spaces. **By leveraging compliant structures, distributed mechanical responses, and continuous contact with the surrounding environment, the next-generation robots can maintain rhythmic movement, actively adjust their postures, and enhance their ability to pass through restricted passages.** These characteristics are particularly important for post-disaster exploration, as robots often need to navigate through narrow gaps, curved passages, uneven surfaces, and spaces with uncertain geometries. **This raises a key question: how can we design a robot that reproduces the efficient and adaptive locomotion strategies of insects in confined spaces?**

2.2 From Air Dancers to Insect-Like Rhythmic Locomotion

Under continuous airflow, the flexible arms of an inflatable dancing figure repeatedly bend, store energy, and rapidly rebound—a periodic motion pattern strikingly similar to the bending-and-extending cycle of the hind legs of insects(see Figure 2-2). During movement, insects first accumulate elastic potential energy by bending their hind limbs, then release this energy through rapid extension to generate the instantaneous forces required for propulsion or jumping. Similarly, the inflatable dancer's arms do not rely on external periodic control but instead spontaneously oscillate and rebound due to the combined effects of continuous airflow, flexible structure, and material elasticity. Although arising from different physical systems, both mechanisms embody a rhythmic actuation process of "bending—energy storage—release—recovery." In fact, the repeated bending and rebounding of the inflatable figure can be viewed as a flow-induced self-excited oscillation resulting from the interaction between continuous airflow and flexible structures. **This phenomenon inspires us: if we could incorporate such a self-generating periodic motion mechanism into robot design, might robots no longer need complex electronic timing controls, but instead produce insect-like rhythmic actuation through their own fluid-structure dynamics?** Furthermore, could we leverage the principle of self-excited oscillation to design a new generation of compact space exploration robots with simpler structures, lower control complexity, and enhanced adaptability to narrow, curved, and irregular environments?

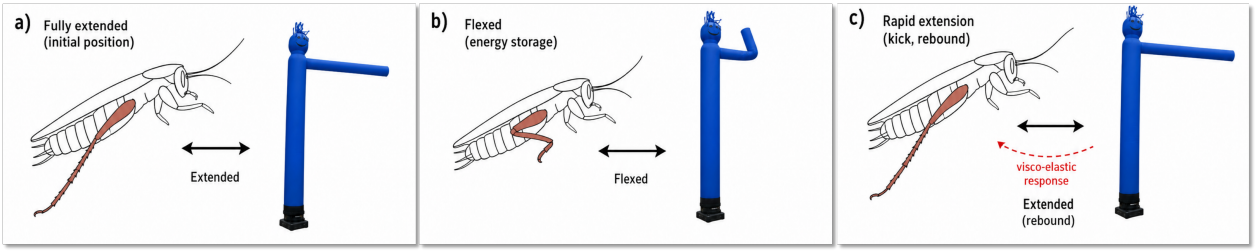


Figure 2-2: Bio-inspired analogy between insect hind-leg motion and the airflow-driven oscillation of an inflatable air dancer.

2.3 The physical principle of self-excited oscillation



Figure 2-3: The self-excited oscillation phenomenon of the soft ring tube [13]

Self-excited oscillation is the phenomenon in which a system generates periodic output through its own dynamic characteristics in response to a non-oscillatory input (such as a constant pressure or flow rate). In fluid drive systems, this phenomenon can be achieved through specific structural designs, particularly through the flat ring tube (FRT) proposed by Tsukagoshi et al. [13].

2.3.1 Self-excited oscillation mechanism of flat ring tube

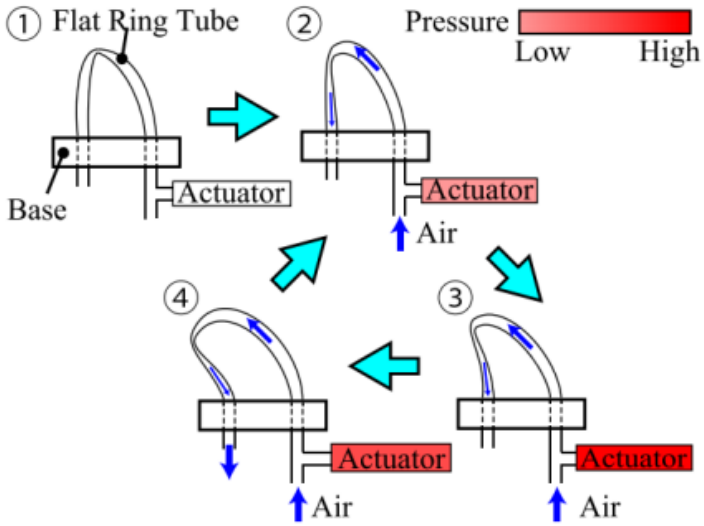


Figure 2-4: The self-excited oscillation process [15]

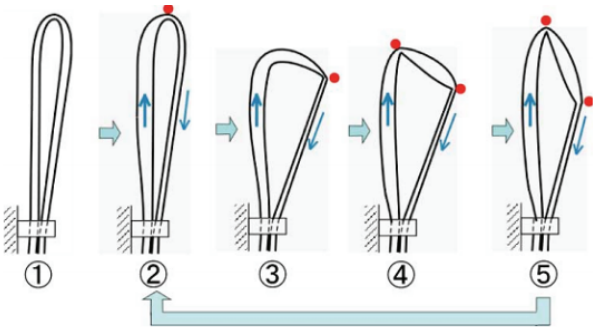


Figure 2-5: A cycle of self-excited oscillation [13]

FRT is a polyurethane flat-section annular pipe. When a fluid with constant pressure enters the pipe, the pipe gradually bends, and when the curvature reaches its limit, the pipe buckles at a point, completely cutting off the fluid passage [13]. As the fluid continues to be pressurized, the buckling point is pushed from upstream to downstream. Meanwhile, a new buckling point is generated on the upstream side, repeating the same trajectory [13,15]. Nabae and Kitamura [15] further explained the working principle of FRT as a self-excited oscillatory valve: during oscillation, the pressure at the FRT inlet changes periodically as the buckling point moves. When the buckling point approaches the inlet, the fluid is blocked, and the pressure increases. When the buckling point is reached, the fluid is released, and the pressure decreases. This pressure fluctuation can directly drive soft actuators and generate periodic motion without electronically timed valve switching.The physical characteristics of self-excited oscillation can effectively mimic the rhythmic movements of insects in nature.

2.3.2 Factors that affect oscillation characteristics

Shown in Figure 2-6, experimental results demonstrate how the frequency is related to the pipe length and flow rate. Experimental studies illustrate that the oscillation frequency of FRT is closely related to the pipe length and flow rate. Under constant flow rate conditions, the oscillation frequency decreases with increasing pipe length. Under constant pipe length conditions, the frequency increases with increasing flow rate [13].

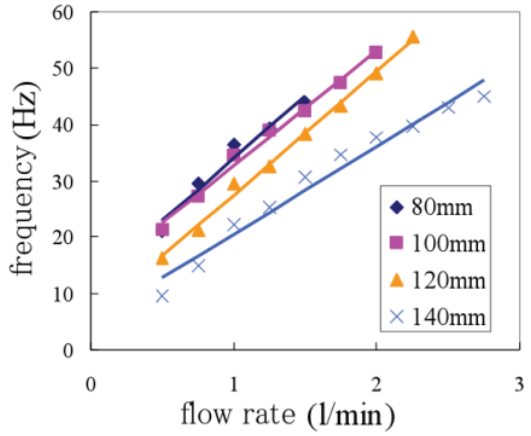


Figure 2-6: A cycle of self-excited oscillation [13]

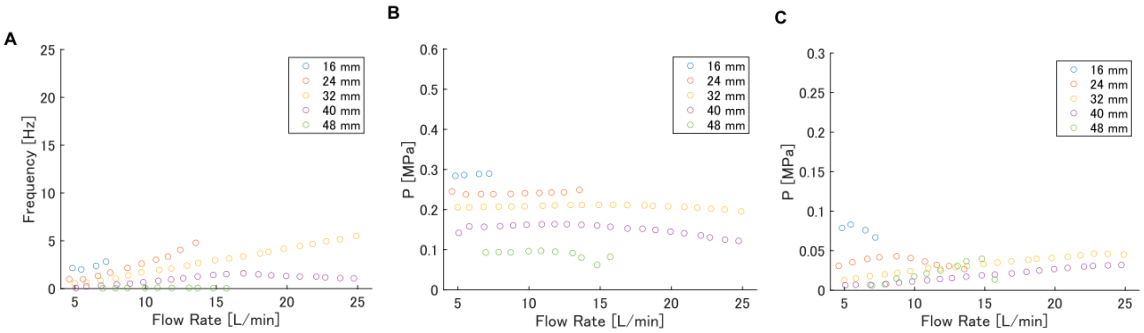


Figure 2-7: The radius of curvature (defined as the distance between two fixed points) influences oscillation characteristics [15].

In addition, systematic experiments by Nabae and Kitamura [15] showed that the radius of curvature of the FRT (determined by the distance between two fixed points) also affects oscillation characteristics: the smaller the radius of curvature, the higher the maximum pressure and the higher the oscillation frequency. This finding provides a crucial basis for the design of structural parameters of self-excited oscillation units.

2.3.3 Mechanical properties and self-excited oscillation of inflatable structures

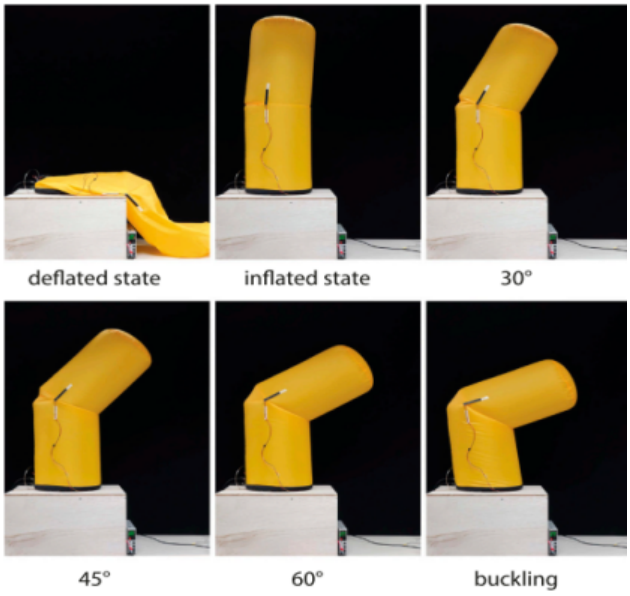


Figure 2-8: A sequence of movement of a blower-driven soft pneumatic joint: deflation, inflation, and flexion [14]

The blower-driven soft pneumatic joint proposed by Niiyama et al. [14] offers a distinct perspective on the mechanical behavior of self-excited oscillating soft limbs. They designed a pneumatic joint with built-in tendons, enabling flexion and extension by controlling internal pressure and tendon tension. Although the study adopted an active control method, the passive recovery behavior of the joint under constant pressure is similar to self-excited oscillation. This research team established a quasi-static theoretical model of the pneumatic joint, highlighting that the joint recovery torque τ is determined by the rate of change of internal pressure P and volume V with angle θ [14]:

$$\tau(\theta) = -P \cdot \frac{dV}{d\theta} \tag{1}$$

This model reveals the key mechanical law of soft pneumatic structures: the joint stiffness can be controlled by internal pressure and geometric parameters. When the rotation axis offset parameters α are relatively small, the joint recovery torque is large. Specifically, when α equals $\pi/2$, the joint has almost no recovery torque and is easy to bend [14]. This theory provides a mechanical basis for the structural design of self-excited oscillating soft limbs.

2.4 Chapter Summary

This chapter establishes the theoretical foundation for a self-excited soft robot designed for post-disaster confined-space search and rescue, focusing on two aspects: bio-inspired locomotion and physical intelligence.

1. Bionic Level: Insects rhythmic movement is achieved through the coordinated action of CPG (rhythm generation), neural feedback (rhythm regulation), and premechanical reflexes (rapid response). This mechanism suggests that we can achieve rhythm-generating functions similar to those of CPGs through physical structures and mechanical feedback mechanisms based on material properties, thereby generating rhythmic motion with reduced dependence on electronic timing control.

2. Physical Principle Level: The self-excited oscillation of the FRT originates from the dynamic coupling of fluid pressure and structural buckling. The tube length and flow rate can control the oscillation frequency. The mechanical model of the inflatable structure further reveals the relationships among internal pressure, geometric parameters, and restoring torque, providing a quantitative basis for the design of self-excited oscillating limbs.

Based on the above principle, **this study further explores whether self-excited oscillation can serve as a feasible and practically applicable motion driving mechanism for robots in narrow spaces after disasters.** The proposed system combines self-excited oscillation based on FRT, compliant soft structure, and differential fluid drive. It achieves basic linear propulsion and active steering while reducing reliance on complex mechanical structures and electronic gait generation systems.

It should be emphasized that the main goal of this research is to verify the feasibility, controllability, and adaptability of self-excited oscillation as a robot driving mechanism. Therefore, the current prototype is only evaluated as a motion platform and does not carry cameras, life detection sensors, environmental sensors, or other loads. After the basic motion mechanism is fully verified, these perception and search functions can be expanded as future research directions.

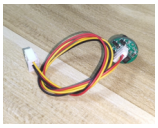
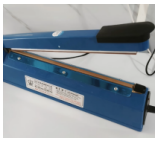
---

3 Design and Implementation of the Self-Excited Oscillation Unit

3.1 Material Selection and Environmental Adaptability

The material selection for the self-excited oscillation unit considers mechanical properties, fabrication feasibility, and environmental adaptability. For post-disaster confined-space search, the materials should be flexible, lightweight, durable, and capable of repeated elastic deformation in narrow, irregular, wet, and dusty environments.

Table 3-1: List of Materials

Name	Photo	Specifications	Function Description
Micro vacuum pump		Voltage: DC 5V Maximum inflation pressure: 60KPa Maximum vacuum pressure: -40KPa Maximum flow rate: 0.8L/min Weight: 15g	The pump provides a continuous pneumatic input for the self-excited oscillation unit. The supplied airflow enables repeated inflation, buckling, pressure release, and elastic recovery of the TPU chamber, thereby supporting continuous oscillatory locomotion.
TPU film		Shore Hardness: 85A, 95A. 0.1mm thickness.	TPU film is the key material used to fabricate the pneumatic oscillation units. Its flexibility, elastic recovery, tear resistance, and heat-sealing capability allow the units to undergo repeated inflation and buckling while maintaining structural integrity. Its compliant surface also improves contact adaptability in narrow and irregular passages.
ESP32 mini		Voltage: DC 5V	The ESP32 mini regulates the electrical input to the air pump during testing and assists in controlling the pump operating condition. By adjusting the pump input, the airflow supplied to the oscillation unit can be changed, thereby influencing its oscillation frequency and stability.
Air Pressure Sensor Module		Pressure detection range: 0-100Kpa	The sensor records the pressure variation inside the pneumatic circuit. The measured pressure-time signal is used to identify oscillation cycles, calculate oscillation frequency, and evaluate the stability of the self-excited oscillation unit.
Heat-sealing machine		20×2mm seal	The heat-sealing machine bonds the folded TPU film layers to form airtight tubular chambers with consistent dimensions. Reliable sealing is necessary for maintaining internal pressure and stable oscillation.

Name	Photo	Specifications	Function Description
Gas flow meter		0.3-3L/min	The gas flow meter measures the airflow rate supplied to the oscillation unit. The measured value is used to establish the quantitative relationship between pneumatic input, oscillation frequency, and pressure variation.
High-flow air pump		15L/min	The high-flow air pump provides an adjustable airflow rate of 0-3 L/min for the parameter-characterization experiments. It is used when the required experimental flow rate exceeds the maximum flow capacity of the compact micro air pump.

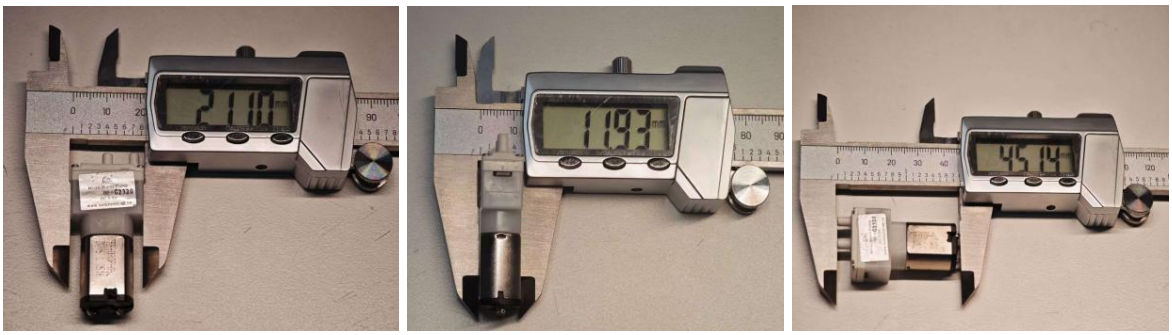


Figure 3-1: Dimensions of the compact micro air pump ($21 \times 12 \times 45$ mm)

Micro vacuum pump: As shown in Figure 3-1, two compact micro air pumps (DC 5 V, maximum flow rate 0.8 L/min, maximum positive pressure 60 kPa) were used in the integrated robot prototype. Each pump independently supplied one self-excited oscillation unit. A separate high-flow air pump was used only in the parameter experiments requiring flow rates above 0.8 L/min.

TPU film: A TPU film with a Shore hardness of 85A and a thickness of 0.1 mm was used as the main structural material. Its flexibility, elastic recovery, tear resistance, and heat-sealing capability allow the oscillation unit to undergo repeated inflation and deformation. These properties also improve its adaptability to narrow and irregular passages.

Auxiliary materials and tools: The auxiliary materials included flexible sealing tape and pneumatic tubes with diameters of 4 mm, 6 mm, and 10 mm. An ESP32 was used to regulate the air-pump input. A heat-sealing machine was used to fabricate the TPU tubes, and a 3D printer was used to produce the air-pump mounting bracket.

3.2 Design of Self-Excited Unit Structure

The design of the self-excited oscillation unit is based on the Flat Ring Tube (FRT) principle proposed by Tsukagoshi et al. [13]. The core mechanism of FRT can be demonstrated by introducing a fluid with constant pressure into the flat cross-section ring tube as the pipe gradually bends. When bending reaches the curvilinear limit, the pipe buckles at a point, and the fluid channel is completely cut off. As the fluid remains pressurized, the buckling point shifts from upstream to downstream, and a new buckling point forms on the upstream side, leading to sustained, periodic oscillation [13,15]. During this process, the inlet pressure fluctuates periodically with changes in the buckling point position. This pressure fluctuation can directly drive the soft actuator and generate periodic motion without electronically timed valve switching [15].

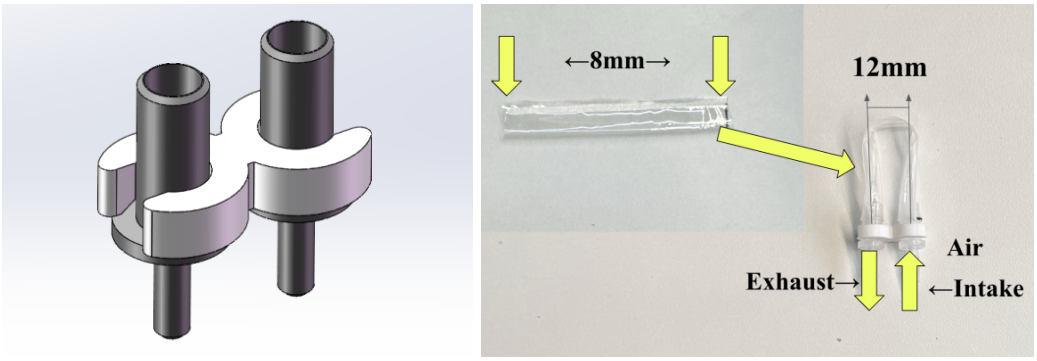


Figure 3-2: The three-dimensional design drawing and the physical prototype

Nabae and Kitamura's research illustrates that the oscillation frequency of FRT is inversely proportional to the tube length and directly proportional to the flow rate [15]. This correlation provides a theoretical basis for the size design of the oscillation unit in this research. By adjusting the length of the TPU thin tube and the air supply flow rate, the oscillation frequency can be controlled to meet the expectations of different motion speeds.

3.3 Design and Fabrication of TPU Tubes

The TPU tube is a crucial actuator of the self-excited oscillation unit, and its geometric parameters and fabrication quality directly influence the stability of the oscillation behavior. This study uses a thermoplastic process to produce TPU tubes with various specifications.



Figure 3-3: 0.1mm thick TPU materal wth a hardness of 85A.

Material preparation: The process involves selecting a 0.1mm-thick TPU film with a hardness of 85A (as shown in Figure 3-3). Then, cut the film into rectangular strips, with the width determined by the target pipe diameter.



Figure 3-4: Fabrication of TPU Tubes using a Thermoforming Machine.

Heat-sealing Process: The TPU film is folded in half and heat-sealed at a set temperature (approximately 160 degree celsius) and pressure using a thermoforming machine to form a tubular structure (as shown in Figure 3-4). By adjusting the width of the heat-sealing mold, thin tubes of different diameters can be prepared. This study prepared three diameter series: 5mm, 10mm, 15mm (Figure 3-5). Different diameters correspond to different bending stiffness and internal cavity volume. It is expected that the smaller the diameter, the greater the bending stiffness and the higher the oscillation frequency. As the diameter increases, so does the volume change and the output force.

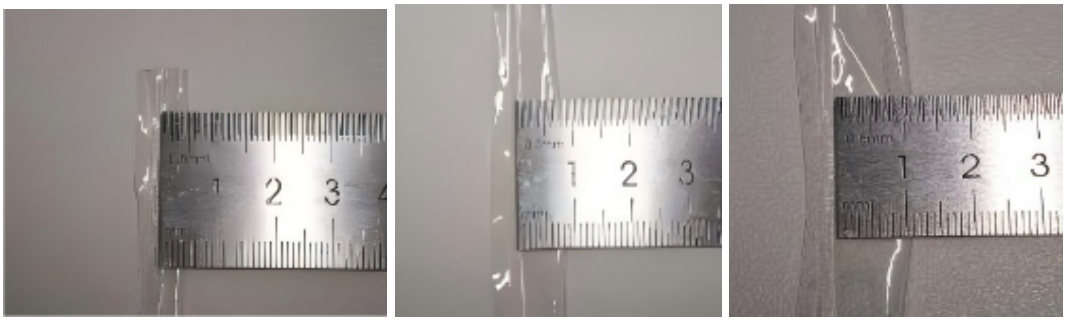


Figure 3-5: Fabrication of TPU Tubes using a Thermoforming Machine.

Tube diameter series: This study fabricated three different diameter TPU thin tubes: 5mm, 10mm, and 15mm (as shown in Figure 3-5). Individual-diameter tubes exhibit different bending stiffness and internal cavity volumes, thereby affecting the oscillation frequency and output force. Smaller-diameter tubes have much greater rigidity and bending stiffness and can generate higher oscillation frequencies. Larger-diameter tubes exhibit greater volume change and can thus generate a greater driving force.

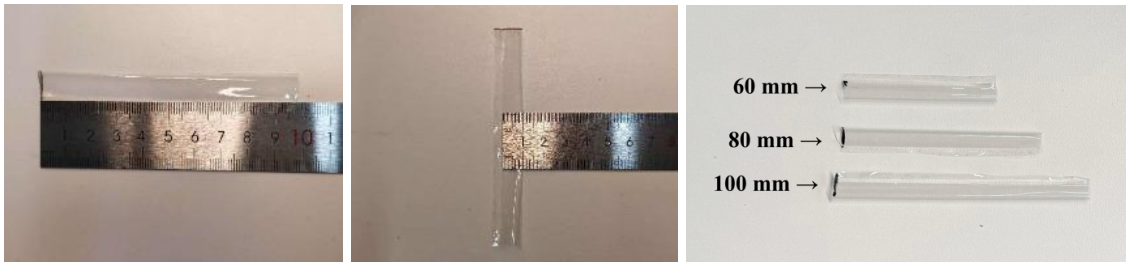


Figure 3-6: Measurement method of TPU thin tubes and display of thin tubes of 60mm, 80mm, and 100mm.

Length series: To systematically explore the influence of length on oscillation characteristics, TPU tubes with lengths of 60mm, 80mm, and 100mm were prepared with a fixed tube width of 10mm (as shown in Figure 3-6). The length range was selected based on the research results of the reference sources [15] to ensure that the oscillation behavior was within the observable range.



Figure 3-7: Bending effect of the TPU tube.

The bending performance test: The prepared TPU thin tube was manually bent (as shown in Figure 3-7), and its recovery behavior after release was observed. The experiment shows that the TPU thin tube with a hardness of 85A exhibits good elastic recovery, quickly returning to its original shape after bending and release. This characteristic is the basis for maintaining stable oscillation.

3.4 Performance Experiment of Self-Excited Oscillation Unit

3.4.1 Experimental Objectives and Design

To verify the basic performance of the self-excited oscillation unit and optimize its design parameters, a series of experiments was conducted to address the following questions:

1. The influence of TPU tube diameter (5, 10, 15mm) and length (60, 80, 100mm) on the oscillation frequency and pressure amplitude.
2. The quantitative relationship between oscillation frequency and air supply flow rate.
3. Determining the optimal unit size suitable for the subsequent robot assembly.

The experimental setup is shown in Figure 3-2 (a schematic diagram added here). The TPU tube was bent into a ring, with the inlet and outlet ends connected. The inlet was connected to a micro air pump, and a flow meter (0.3-3 L/min) and a pressure sensor (0-100 kPa) were connected in series. The outlet was kept open. The flow rate was adjusted by varying the air pump power. After the oscillation stabilized, the inlet pressure waveform was collected by the pressure sensor at a sampling frequency of 100 Hz. At least 20 complete cycles were recorded for each condition.

3.4.2 Frequency Extraction Method

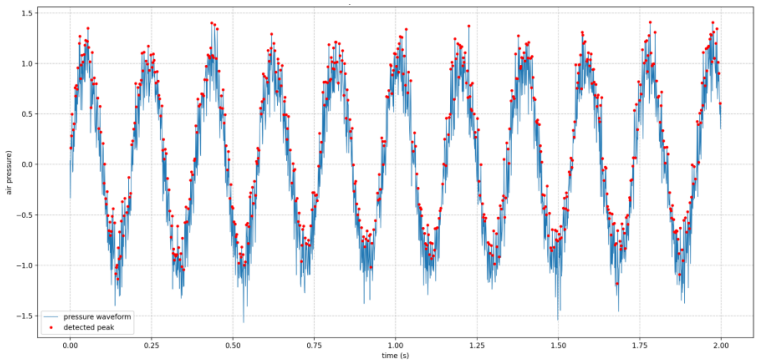


Figure 3-8: Frequency estimation using the time-domain periodic method.

The oscillation frequency is calculated using the time-domain periodic method: the acquired pressure-time waveform is imported into Python, a peak-detection algorithm identifies the pressure peak in each cycle, the time interval $\triangle t$ between adjacent peaks is calculated, and the instantaneous frequency $f = 1/\triangle t$ is determined. The average value of 20 consecutive cycles is taken as the oscillation frequency under this condition.

3.4.3 Results and Analysis

1. Influence of Pipe Length on Oscillation Frequency

Table 3-2: FRT State Before and After Valve Opening

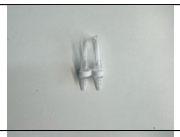
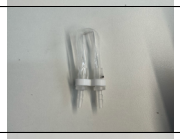
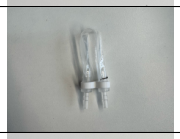
L	First Position	Middle Pressure	Before pressure release	After pressure release
60mm				
80mm				
100mm				

Table 3-3: Oscillation frequencies of three pipe lengths (60, 80, 100 mm) at different flow rates

Flow rate (L/min)	60 mm frequency (Hz)	80 mm frequency (Hz)	100 mm frequency (Hz)
0.4	1.96	4.15	1.22
0.8	8.47	5.23	6.50
1.2	9.79	8.22	7.58
1.6	17.69	10.34	6.64
2.0	17.77	11.45	12.21
2.4	21.74	14.28	15.02
2.8	24.21	17.78	12.36

Table 3-3 summarizes the oscillation frequencies of three pipe lengths (60, 80, and 100 mm) at different flow rates. Figure 3-9 shows the frequency-flow rate relationship curve with an 80 mm pipe length as an example. The overall trend is consistent with the description in reference [15]: at the same pipe length, the frequency increases with increasing flow rate; at the same flow rate, the frequency decreases with increasing pipe length.

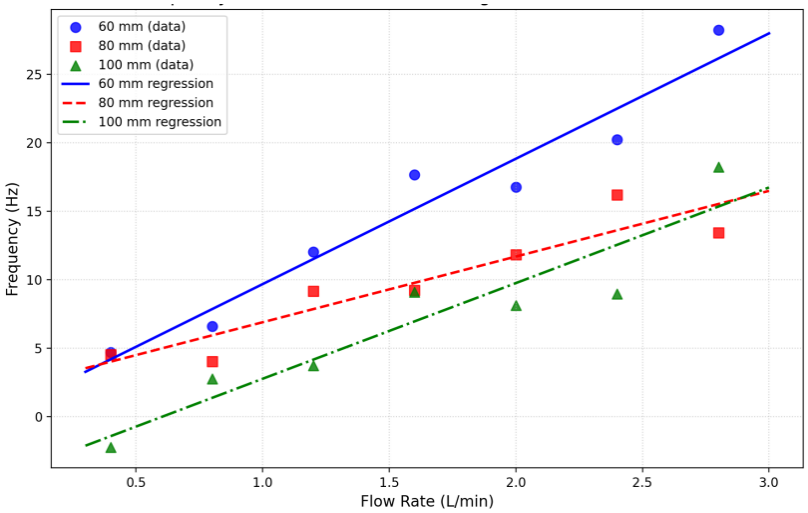


Figure 3-9: Relationship between pipe length, width, and flow rate (pipe length 80 mm)

However, an anomaly was observed at low flow rates (0.4 L/min): the frequency of the 80 mm tube (4.15 Hz) was higher than that of the 60 mm tube (1.96 Hz). This phenomenon may be related to the "dead zone" behavior of buckling point movement at extremely low flow rates. For the shorter 60 mm tube, its bending stiffness is greater, and the buckling pressure required to initiate movement is higher. Therefore, at low flow rates, intermittent oscillations or extremely small oscillation amplitudes may occur, leading to a lower effective frequency. The 80 mm tube, with its moderate stiffness, can maintain a more consistent buckling-point movement at the same low flow rate, thereby exhibiting a higher oscillation frequency. When the flow rate increases (¿0.8 L/min), the frequency of the 60 mm tube quickly surpasses that of the 60 mm tube, consistent with theoretical expectations. This phenomenon suggests that, in low-drive-power scenarios, shorter tube length is not always better; there is an optimal length range to ensure oscillation reliability.

2. The Influence of Pipe Diameter (Width) on Oscillation Frequency

Table 3-4: Relationship between Frequency, Width, and Flow Rate (Pipe Length 80 mm)

Flow rate (L/min)	Width 5 mm Frequency (Hz)	Width 10 mm Frequency(Hz)	Width 15 mm Frequency (Hz)
0.4	6.05	0.76	0.66
0.8	11.35	5.21	4.27
1.2	15.25	9.53	4.02
1.6	23.02	11.22	7.17
2.0	25.97	13.10	6.34
2.4	31.59	11.73	10.90
2.8	31.98	17.77	12.70

Table 3-4 and Figure 3-10 show the frequency-flow rate relationship for different pipe diameters (5, 10, and 15 mm) with a fixed pipe length of 80 mm. Experimental data show that at the same flow rate, the smaller the pipe diameter, the higher the oscillation frequency. For example, at a flow rate of 2.0 L/min, the frequency of the 5 mm pipe is 25.97 Hz, while that of the 15 mm pipe is only 6.34 Hz. Fluid mechanics and structural mechanics can explain this result: smaller diameter pipes have smaller cross-sectional areas, higher fluid velocities, and a faster establishment of pressure differential before and after the buckling point;

simultaneously, smaller diameter pipes have greater bending stiffness, requiring a stronger elastic restoring force to recover their original shape after buckling, thus shortening the oscillation period.

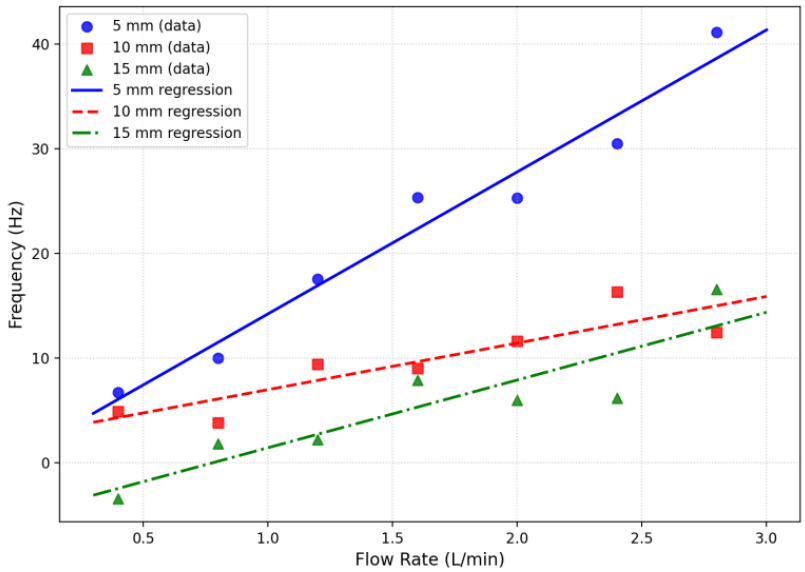


Figure 3-10: Relationship between frequency, width, and flow rate (pipe length 80 mm)

It is worth noting that while the 5 mm tube has a high frequency, its small internal volume limits the volume of gas expelled with each oscillation, which may not provide sufficient driving force for limb movement. Conversely, the 15 mm tube has a large output force but a low frequency, which is not conducive to achieving smooth movement. Therefore, a trade-off must be struck between frequency and output force.

3. Oscillation pressure amplitude

The pressure amplitude (the difference between the maximum and minimum values) decreases with increasing pipe length and increases with increasing pipe diameter. Longer pipes have greater flexibility and release pressure more fully when bent, resulting in a lower minimum pressure and a smaller pressure amplitude. Larger pipe diameters allow for greater gas accumulation, leading to higher maximum pressure and larger amplitudes. This trend is consistent with the observations in reference [15].

3.4.4 Determination of Unit Size

Considering the overall size constraints of the robot, the required movement speed, and the balance of driving force, the following parameters were selected as the standard unit for subsequent integration into the whole machine:

Pipe width (diameter): 10 mm (balancing high frequency and sufficient output force)

Pipe length: 80 mm (stable oscillation within the commonly used flow rate range of 0.8–1.2 L/min, with a frequency of approximately 5–8 Hz, suitable for walking motion)

Air supply flow rate: 0.8 L/min

3.5 Chapter Summary

This chapter completed the material selection, structural design, fabrication, and performance characterization of the self-excited oscillating soft limb. Through a series of experiments, the effects of TPU tube length and diameter on oscillation frequency and pressure amplitude were systematically analyzed, and empirical relationships between frequency, flow rate, and geometric parameters were obtained. Experimental results show that the oscillation frequency increases with increasing flow rate and decreases with increasing tube length and diameter; a tube-length-dependent oscillation initiation threshold exists in the low-flow-rate range.

Based on the experimental results, the unit size (10 mm wide, 80 mm long) suitable for the entire robot was determined, laying the foundation for subsequent multi-limb coordinated motion. The next chapter will introduce the robot's system integration and its adaptability to post-disaster confined-space environments.

4 Robot System Integration and Confined-Space Adaptation

In Chapter 3, we determined the dimensions (10 mm wide and 80 mm long) and driving parameters (flow rate of 0.8 L/min and oscillation frequency of approximately 5.2 Hz) of the self-excited oscillation unit. Based on these parameters, this chapter integrates the complete robot and evaluates its motion performance in confined passages. The experiments mainly examine whether two self-excited oscillation units can generate stable forward motion and whether differential airflow can be used to achieve steering.

4.1 Overall Mechanical Integration of the Robot

4.1.1 Mechanical Structure Design



Figure 4-1: Modeling with SolidWorks and measuring the dimensions of a miniature air pump using vernier calipers.

To achieve miniaturization and integration, the core power components were first precisely modeled. The dimensions of the miniature vacuum pump were measured using calipers to be 21 mm × 12 mm × 45 mm (Figure 4-1). Based on these dimensions, a dedicated mounting bracket was designed in SolidWorks (Figure 4-2). The bracket, made of PLA material using fused deposition modeling 3D printing, securely holds the pump motor and includes pre-drilled mounting holes for connection to the robot's body.

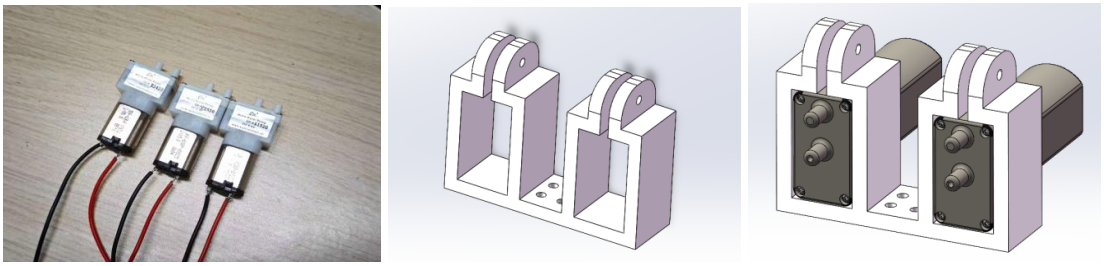


Figure 4-2: Design of a bracket for a miniature air pump motor

The robot's overall structure adopts a circumferentially distributed limb layout, with two self-excited oscillating units symmetrically distributed around the central axis at 180° (Figure 4-3). The advantages of this layout are: Multi-limb coordination: Alternating oscillation of the two units generates a more stable gait;

Confined-passage adaptation: The circumferential distribution helps the robot maintain its position inside narrow passages.

Differential steering: Deflection motion can be achieved by independently adjusting the airflow supplied to each oscillation unit.

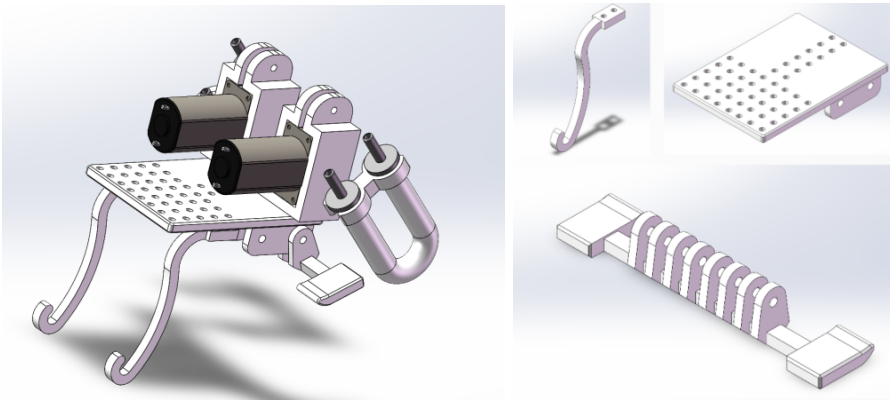


Figure 4-3: Overall structural design of the self-oscillating robot

Figure 4-3 shows the 3D design drawings of the robot. The design adopts a circumferentially distributed limb layout, with two self-excited oscillating units evenly distributed around the central axis. The advantages of this layout are:

- Multi-limb collaboration can generate a more stable gait.
- The circumferential distribution helps the robot maintain its position inside narrow confined passages.
- The fluid network allows the airflow supplied to the two oscillation units to be adjusted independently.

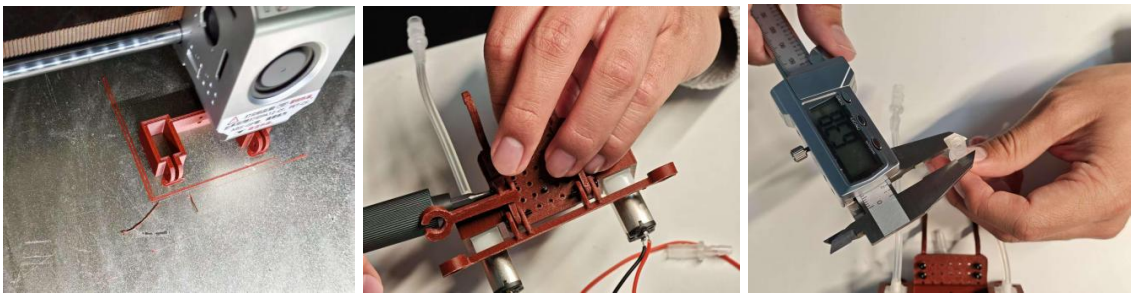


Figure 4-4: 3D-printed parts and structural adjustment details

Figure 4-4 illustrates the assembly process and structural adjustments of the 3D-printed parts. Two micro air pumps are mounted in the central bracket. Each pump is directly connected to one self-excited oscillation unit, forming two independent pneumatic branches. A manual throttle valve is installed in each branch to adjust the airflow supplied to the corresponding unit. The two pumps and their pneumatic connections are integrated into the central robot body, forming a compact drive system (Figure 4-5).

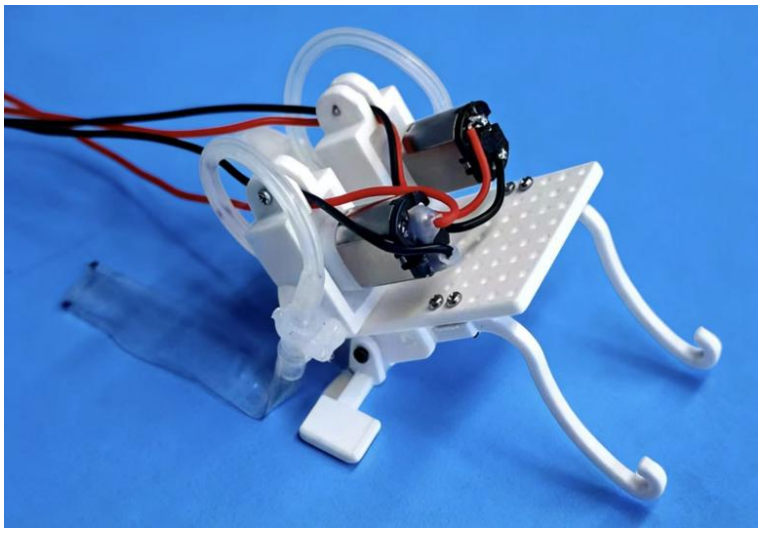


Figure 4-5: Physical demonstration of the self-oscillating robot.

The robot's final dimensions are 136 mm long, 76 mm wide, and 60 mm high (Figure 4-6). Two self-excited oscillation units (TPU thin tubes) are located on both sides and connected to the central rigid frame via flexible connectors. The air outlets of the thin tubes are open to the atmosphere to ensure periodic gas emission during oscillation.

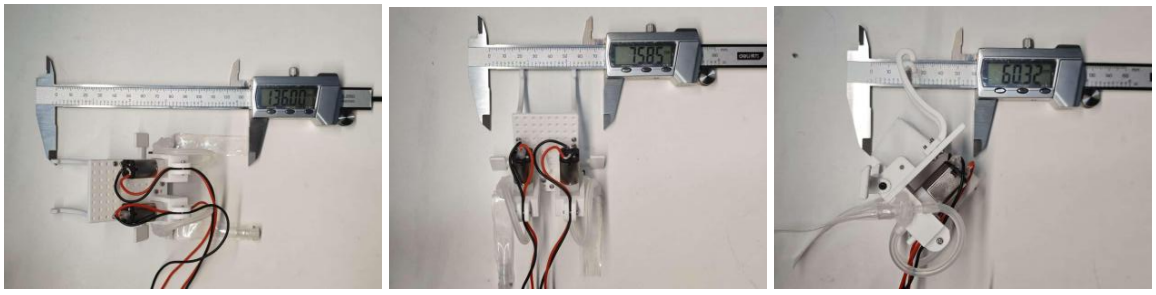


Figure 4-6: The self-oscillating robot is 136mm long, 76mm wide, and 60mm high.

4.1.2 Gait Generation Mechanism

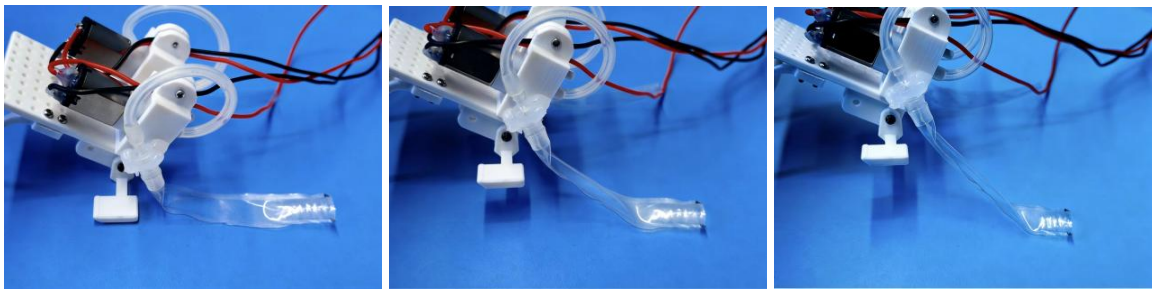


Figure 4-7: 3D printed parts and structural adjustment details

The design of the fluid network is crucial for achieving differential steering. As shown in Figure 4-7, each self-excited oscillation unit is supplied with air through an independent micro-pump. Throttling valves allow manual adjustment of the flow rate in that branch, thereby changing the oscillation frequency and output force of the corresponding unit. When the flow rates on both sides are equal, the two units operate at similar

oscillation frequencies, and the robot moves forward in a straight line; when the flow rate on the left side is greater than that on the right, the output force of the left unit increases, generating a yaw torque, and the robot turns to the right; conversely, the flow rate on the left side is less than that on the right.

Axial motion mode: The throttle valves on both sides are opened to the same degree, and the two self-excited oscillation units operate at similar frequencies of approximately 5.2 Hz.. When the unit inflates, the limb bends backward and downward, applying a backward oblique force to the ground or passage wall, propelling the robot forward; when the unit deflates and contracts, the limb returns to its original position, completing one motion cycle. Due to the approximately balanced propulsion generated by the two units, the net thrust is forward along the axial direction, resulting in linear motion.

Steering motion mode: Reducing the opening of the throttle valve on one side reduces the airflow rate supplied to the unit on that side. Based on the findings in Chapter 3, a decrease in flow rate results in a lower unit oscillation frequency, a reduced pressure amplitude, and a weaker output force. The difference in output force between the two sides generates a yaw torque about the robot's center of gravity, causing it to turn toward the side with the weaker output force. By adjusting the flow rate difference between the two sides, the turning radius and angular velocity can be controlled.

4.2 Experimental Verification of Motion Performance

To verify the robot's motion capabilities, two quantitative experiments were conducted under ground conditions: axial propulsion and steering control. The air supply flow rate was uniformly set to 0.8 L/min (at this flow rate, the oscillation frequency of an 80 mm-long unit is approximately 5.2 Hz). All experiments were repeated five times, and the average value was taken as the final result.

4.2.1 Axial thrust capability test experiment

Experimental Objective: To quantify the linear forward speed and stepping consistency of a robot on a flat, hard surface.

Experimental Method: The robot was placed on a horizontal acrylic plate, and the air pump was started to provide a stable air supply. The robot's motion was recorded with a mobile phone camera (60 fps), and the robot's head position was extracted every 2 seconds using image analysis software. This recording was continued for 10 seconds to obtain the displacement-time curve.

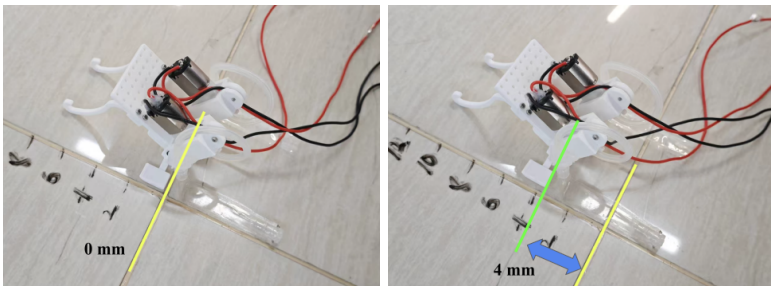


Figure 4-8: Axial propulsion of the robot (measured movement of approximately 4 mm in 10 seconds).

Experimental Results: Figure 4-8 shows the robot's displacement over 10 seconds in one experiment. Table 4-1 summarizes the cumulative displacement data for each 2-second interval across the five experiments, and Table 4-2 shows the corresponding instantaneous velocities. The average total displacement over 10 seconds was 4.18 mm (average of 5 experiments), and the average forward velocity was 0.418 mm/s. The movement was continuous and smooth, without significant pauses or jitter. Based on an oscillation frequency of 5.2 Hz, the average step distance per movement cycle was approximately 0.080 mm (4.18 mm / ($5.2Hz \times 10s$)). The smaller step distance is due to, under ground conditions, the thrust generated by limb bending being partially consumed in overcoming its own gravity, and to a low adhesion coefficient with the ground, resulting in lower-than-expected actual propulsion efficiency.

Table 4-1: Cumulative Displacement Data from Axial Propulsion Experiments (Unit: mm)

Cumulative displacement (mm)						
Time (s)	Group 1	Group 2	Group 3	Group 4	Group 5	Average
0	0.0	0.0	0.0	0.0	0.0	-
2	0.8	0.8	0.9	0.8	0.9	-
4	1.6	1.7	1.7	1.6	1.8	-
6	2.4	2.5	2.6	2.5	2.7	-
8	3.3	3.4	3.4	3.3	3.5	-
10	4.1	4.2	4.2	4.1	4.3	4.18

Table 4-2: Instantaneous velocity data from the axial propulsion experiment (Unit: mm/s)

Instantaneous speed (mm/s)						
Time (s)	Group 1	Group 2	Group 3	Group 4	Group 5	Average
0	-	-	-	-	-	-
2	0.38	0.42	0.43	0.39	0.44	0.41
4	0.40	0.45	0.41	0.40	0.46	0.42
6	0.41	0.42	0.44	0.45	0.47	0.44
8	0.43	0.43	0.39	0.40	0.41	0.41
10	0.39	0.41	0.40	0.42	0.43	0.41

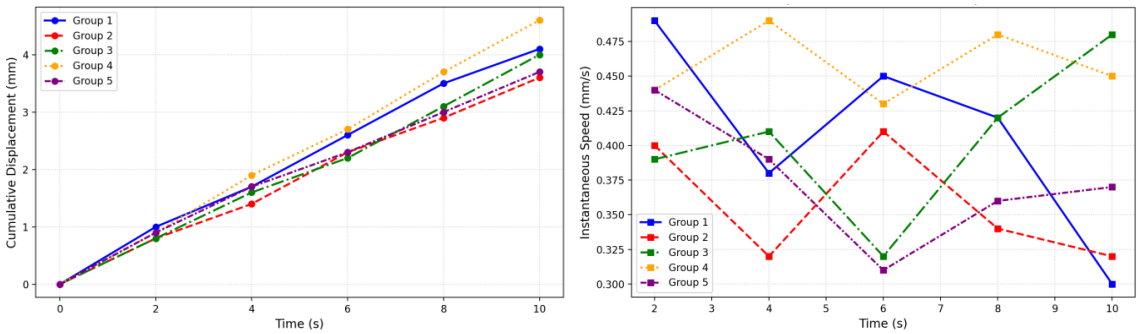


Figure 4-9: Displacement and velocity curves

Figure 4-9Figure 4-9 shows the curves of displacement and velocity as a function of time. The displacement increases approximately linearly, while the velocity remains stable at 0.41–0.44 mm/s, confirming the uniformity of the motion.

4.2.2 Steering Ability Test Experiment

Experimental objective: To quantify the robot's turning angular velocity and control sensitivity.



Figure 4-10: Steering ability test (actual measurement: approximately 23 degrees rotation in 10 seconds)

Experimental Method: Initially, the openings of both throttle valves were set to the same value, and the robot moved in a straight line. At t=0, the opening of the right throttle valve was reduced to 0, keeping the flow rate on the right side constant. A high-speed camera recorded the robot's head trajectory, extracting the robot's orientation angle (relative to the initial direction) every 2 seconds. This recording lasted 10 seconds.

Experimental Results: Figure 4-10Figure 4-10 shows the robot turning over in 10 seconds during a single experiment. Table 4-3 summarizes the cumulative turning angles every 2 seconds for the five experiments, and Table 4-4 shows the corresponding instantaneous angular velocities. The average cumulative turning angle over 10 seconds was 23.3°, and the average angular velocity was 2.33°/s. The turning process was smooth, without overshoot or oscillation. This result demonstrates that effective directional control can be achieved through unilateral airflow throttling.lectronically controlled steering scheme.

Table 4-3: Cumulative Angle Data from Steering Experiments (Unit: °)

Angle (°)						
Time (s)	Group 1	Group 2	Group 3	Group 4	Group 5	Average
0	0.0	0.0	0.0	0.0	0.0	-
2	3.4	4.8	5.7	4.3	5.3	-
4	7.2	9.6	11.9	9.4	9.9	-
6	14.1	14.0	18.2	15.2	13.5	-
8	18.9	18.2	21.8	20.3	17.6	-
10	23.2	22.9	24.5	24.1	21.8	23.3

Table 4-4: Instantaneous angular velocity data from the steering experiment (unit: °/s)

Angular velocity(°/s)						
Time (s)	Group 1	Group 2	Group 3	Group 4	Group 5	Average
0	-	-	-	-	-	-
2	1.71	2.39	2.86	2.15	2.63	2.35
4	1.90	2.42	3.07	2.55	2.31	2.45
6	3.43	2.21	3.15	2.93	1.80	2.70
8	2.43	2.07	1.79	2.54	2.06	2.18
10	2.16	2.38	2.72	2.58	2.10	2.39

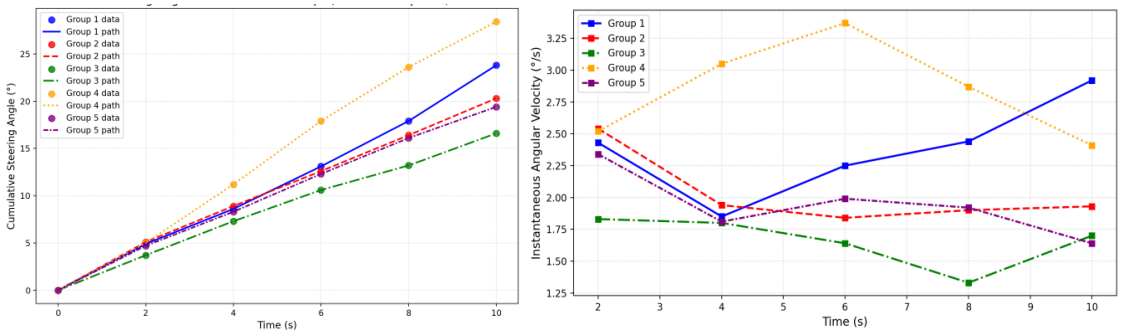


Figure 4-11: Curves of angle and angular velocity

Figure 4-11 shows the curves of angle and angular velocity changing with time. The angle increases approximately linearly, and the angular velocity remains stable at 2.2–2.7°/s, indicating that the steering motion is uniform and controllable.

4.3 Environmental Adaptability Experiment

4.3.1 Motion Performance in Confined Passages of Different Diameters

Experimental objective: To evaluate the robot's motion performance and adaptability in confined passages with different diameters.

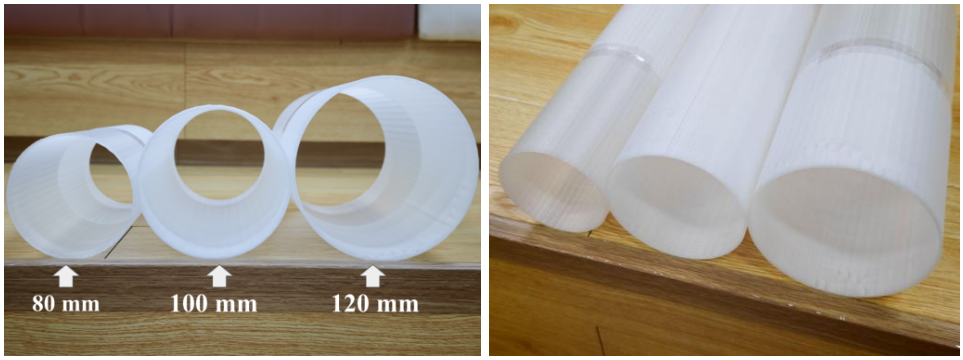


Figure 4-12: Experimental passages with inner diameters of 80 mm, 100 mm, and 120 mm

Experimental Methods: Three acrylic tubes with inner diameters of 80 mm, 100 mm, and 120 mm were

used as standardized confined passages (Figure 4-12). The inner surfaces were tested under both dry and wet conditions. Glycerin was sprayed on the inner surfaces to create a repeatable low-friction wet environment. Wet conditions may occur in post-disaster spaces because of rainfall, firefighting water, damaged pipelines, or underground seepage.

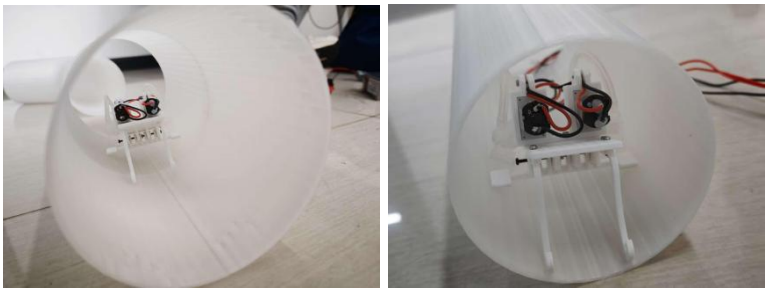


Figure 4-13: Movement effect of a self-oscillating robot inside a pipe.

Experimental results: As shown in Table 4-5, under dry conditions, the velocity decreased with decreasing pipe diameter: 0.42 mm/s in a 120 mm pipe diameter, 0.38 mm/s in a 100 mm pipe diameter (retention rate 90%), and further decreased to 0.30 mm/s in an 80 mm pipe diameter (retention rate 71%). Under wet conditions, the velocities of all pipe diameters were lower than those under dry conditions: 0.38 mm/s in a 120 mm wet condition (retention rate 90%), 0.34 mm/s in a 100 mm wet condition (retention rate 81%), and 0.27 mm/s in an 80 mm wet condition (retention rate 64%). This phenomenon contradicts the intuitive expectation of "lubrication reducing drag." Analysis suggests that while the wet lubricant reduces frictional resistance, it also reduces the adhesion coefficient between the limb and the pipe wall, thereby consuming some of the propulsive force generated during limb bending and failing to be effectively converted into forward motion. Especially in smaller pipe diameters (80 mm), the contact pressure between the limb and the pipe wall is greater, the slippage effect is more pronounced, and the speed decreases the most (from 0.30 mm/s to 0.27 mm/s). Figure 4-13 shows a typical posture of the robot as it moves inside the pipe.

Table 4-5: Motion speed under different pipe diameters and surface conditions

Diameter (mm)	Surface condition	Mean velocity (mm/s)	Speed retention rate (%)
120	Dry	0.42	100
120	Moist	0.38	90
100	Dry	0.38	90
100	Moist	0.34	81
80	Dry	0.30	71
80	Moist	0.27	64

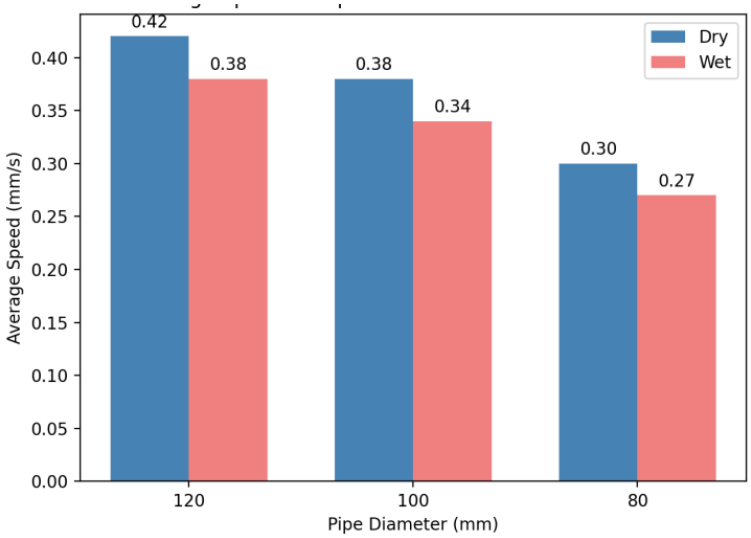


Figure 4-14: Movement effect of a self-oscillating robot inside a pipe.

Referring to Figure 4-14, the robot could pass through confined passages with diameters ranging from 80 to 120 mm, although its speed decreased under wet conditions. When the passage diameter approached the robot's width of 76 mm, increased contact and slippage further reduced its movement speed. These results demonstrate the basic feasibility of the robot in narrow and wet passages. Further experiments in irregular rubble environments will be conducted to evaluate its adaptability under more realistic post-disaster conditions.

4.4 Chapter Summary

This chapter completes the system integration and performance verification of the dual-unit self-excited oscillating soft robot. The main conclusions are as follows:

- Mechanical Integration: A circumferentially distributed dual-unit robot was designed and manufactured. Each oscillation unit was driven by an independent micro air pump, and its airflow rate was adjusted using a separate manual throttle valve.
- Axial Motion: Under ground conditions, the robot's average forward speed was 0.418 mm/s, with smooth, continuous motion and a linear displacement-time relationship.
- Steering Control: Stable deflection motion was generated through unilateral throttling, with an average steering angular velocity of 2.33°/s.
- Environmental Adaptability: The robot could pass through standardized confined passages with diameters ranging from 80 to 120 mm. Under wet conditions, its speed decreased because of increased slippage, but the robot still maintained its passage capability.

The experimental results in this chapter provide a foundation for the comparative and environmental experiments presented in Chapter 5. The next chapter compares the proposed robot with a traditional pneumatic peristaltic robot and further evaluates its performance in a simulated post-disaster rubble environment.

5 Comparative Experiments and Post-Disaster Environment Validation

To evaluate the performance of the self-excited oscillation robot in confined-space applications, a traditional pneumatic peristaltic robot was introduced as the control group. The two robots were compared in terms of

axial motion, curved-passage performance, and control complexity. A simulated rubble-search experiment was also conducted to evaluate the feasibility of the proposed robot in a preliminary post-disaster environment.

5.1 Design and Fabrication of the Airbag Robot

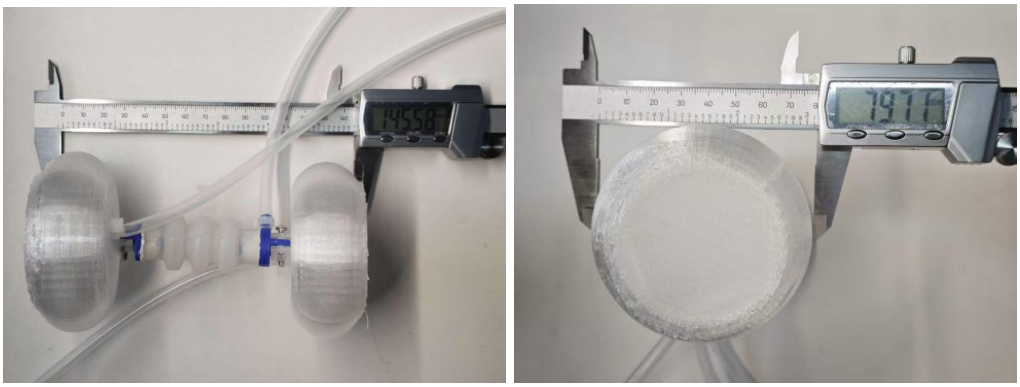


Figure 5-1: The traditional airbag-type peristaltic robot has a length of 146mm and a diameter of 79mm.

Traditional airbag-type peristaltic robots (Figure 5-1) mimic the movement pattern of inchworms and are usually composed of two anchoring airbags (front and rear) and an axially telescopic airbag [**?**]. The working principle is as follows: the rear airbag expands and anchors, and the axial airbag extends to push the front airbag forward; the front airbag expands and anchors, the rear airbag contracts, and the axial airbag shortens to pull the rear airbag forward, completing one peristaltic cycle. This movement method has a simple structure and intuitive control and is commonly used in pneumatic soft robots designed for confined passages.

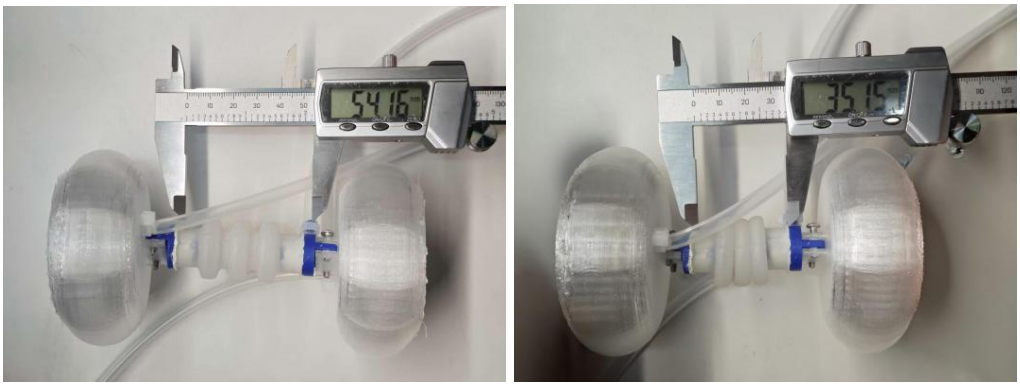


Figure 5-2: The peristaltic step length of a traditional airbag-type peristaltic robot is approximately 9 mm.

To make a fair comparison with the self-excited oscillation robot in this study, we fabricated a bladder-type peristaltic prototype machine based on the design in reference [**?**] (Figure 5-2). The main body is also made of 85A TPU film, and three independent air bladders are heat-sealed: a front anchoring air bladder (diameter 79 mm, length 30 mm), a rear anchoring air bladder (same size), and an axial telescopic air bladder (diameter 15 mm, length 60 mm). The three air bladders are connected to independent solenoid valve groups via 4 mm-diameter air tubes, and inflation and deflation are controlled by the microcontroller (ESP32) according to the preset timing sequence. The air source is the same micro-vacuum pump (maximum pressure of 60 kPa) as the self-excited oscillation robot. This control method requires six solenoid valves and a preset timing program, whereas the self-excited oscillation robot generates periodic motion without electronically timed valve switching. The robot has an overall length of 146 mm and a maximum diameter of 79 mm (Figure 5-1).



Figure 5-3: Traditional airbag-type peristaltic airbag expansion and contraction to assist movement.

During the peristaltic cycle, by adjusting the throttle valve to maintain a moderate degree of airbag inflation, the measured single-step forward distance was approximately 9 mm (5-3). The robot's control requires 6 solenoid valves and 1 microcontroller, making it a typical electronic control system.

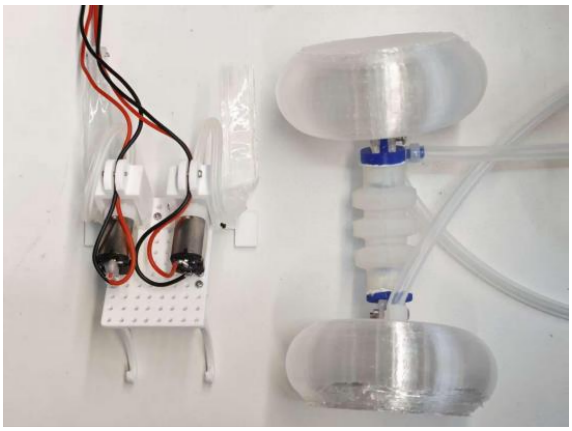


Figure 5-4: Comparison between traditional pneumatic peristaltic robots and self-oscillating robots.

5.2 Comparative Experiment of Axial Motion Capabilities of Airbag Robot and Self-Excited Oscillating Robot in Straight Pipeline

Experimental objective: To quantitatively compare the forward speed and motion stability of two robots in the same straight pipe. Experimental Method: A transparent acrylic straight pipe with an inner diameter of 120 mm and a length of 300 mm was used as the test environment (Figure 5-5). The inner wall of the pipe was kept dry. The robot was placed at the pipe inlet, and the time required from startup to complete passage through the pipe was recorded. The self-excited oscillating robot used an air supply flow rate of 0.8 L/min (corresponding to an oscillation frequency of 5.2 Hz), and the airbag robot used the same air source pressure (20 kPa) and operated according to a preset peristaltic sequence. Each type of robot was tested 5 times.

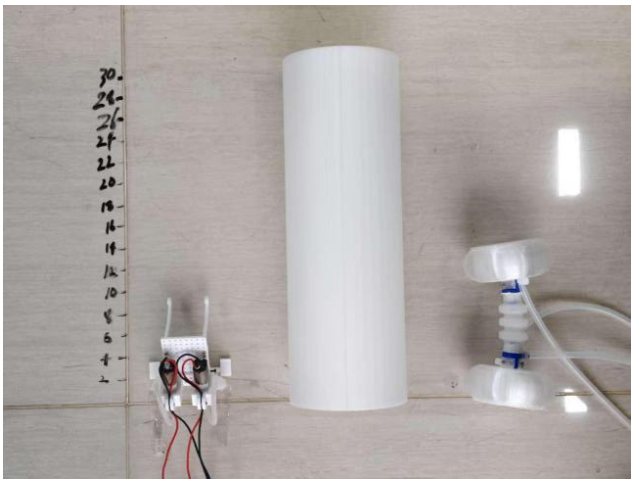


Figure 5-5: Comparative experiment on axial movement capability of a 300mm long pipe (120mm in diameter).

Table 5-1: Comparison of travel time and speed in a straight pipe (300 mm)

Number of experiments	The self-excited oscillation robot travel time (s)	Airbag robot travel time(s)
1	690	1480
2	715	1520
3	740	1650
4	685	1710
5	740	1440
Average	714 ± 28	1560 ± 112
Mean velocity (mm/s)	0.42	0.19

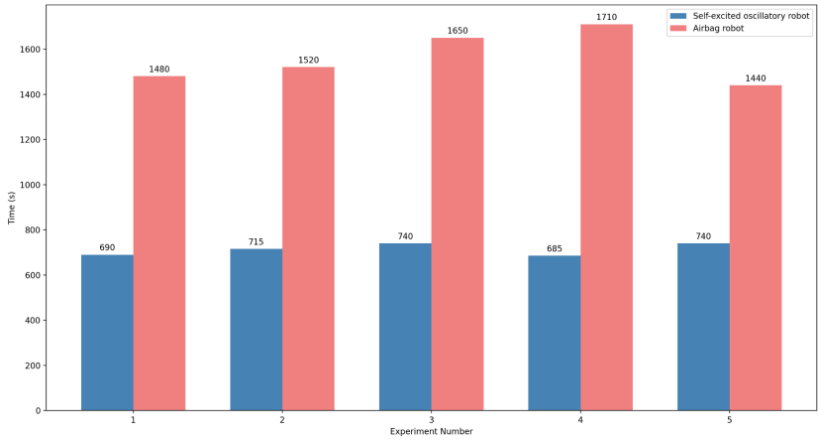


Figure 5-6: Comparison of time and speed for a straight pipe (300 mm)

Experimental Results: Table 5-1 summarizes the transit-time data for the two robots in a 300 mm straight pipe. Combined with the observations in Figure 5-6, the average transit time of the self-excited oscillating

robot in five experiments was 714 s, with a standard deviation of ±28 s and an average speed of 0.42 mm/s. The average transit time of the airbag robot was 1560 s, with a standard deviation of ±112 s and an average speed of 0.19 mm/s, approximately 45% of that of the self-excited oscillating robot. In terms of motion stability, the self-excited oscillating robot exhibited continuous uniform motion; the airbag robot showed obvious stepping motion, with each peristaltic cycle including forward and pause phases, and the displacement curve was stepped. Regarding control complexity, the self-excited oscillation robot used an air pump and two manual throttle valves without requiring electronic timing control or solenoid-valve switching. In contrast, the airbag robot required six solenoid valves, one microcontroller, and supporting circuitry.

5.3 Comparative Experiment in a Curved Pipe

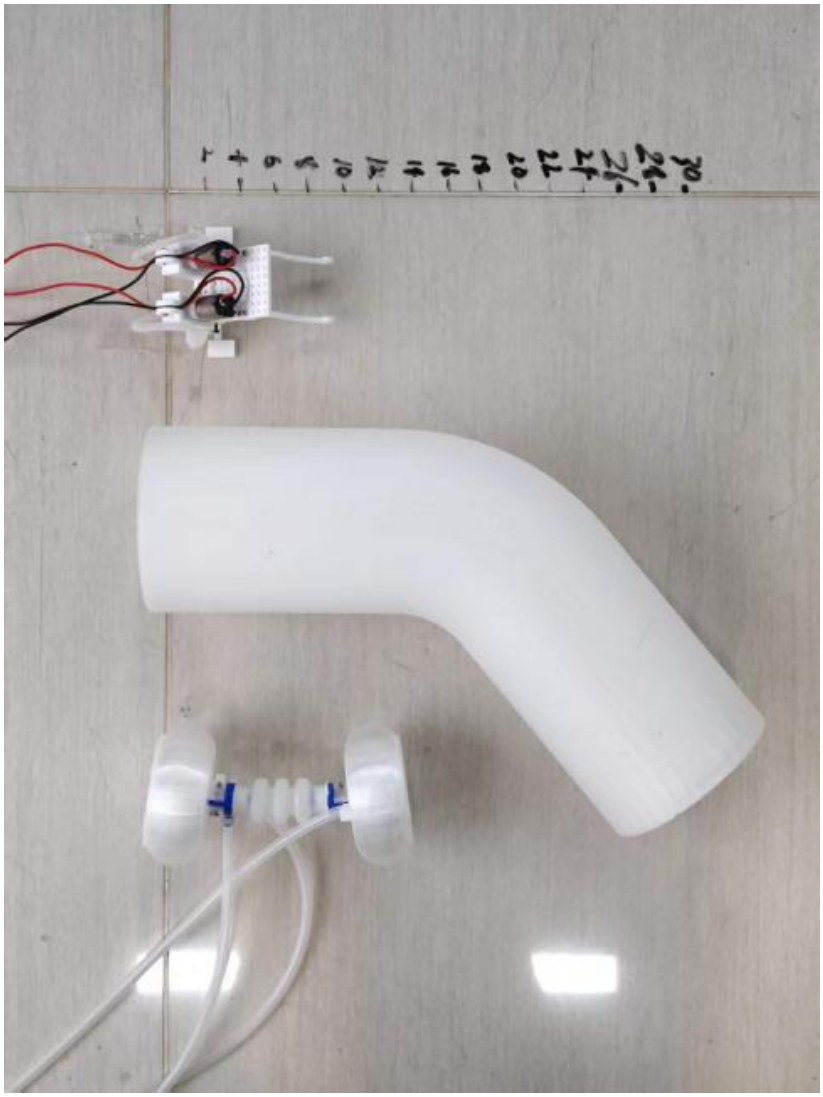


Figure 5-7: Comparison experiment on the turning ability of a 150° angled pipe (100mm in diameter).

Experimental objective: To compare the steering ability and passage efficiency of the two robots in a curved confined passage. The airbag robot lacks an active steering mechanism and can only adapt passively to the pipe's curves; the self-excited oscillating robot can actively adjust its direction through unilateral throttling.

Table 5-2: Comparison of passage time and success rate for bending pipes (150° bend)

Number of experiments	The self-excited oscillation robot passage time(s)	Airbag robot passagel time(s)	Whether there are stoppings/stuck during the airbag robot's maneuvers
1	910	1980	Yes (slight, can be passed with assistance)
2	925	2450	Yes (completely stuck)
3	965	2150	No
4	890	2080	No
5	960	2410	Yes (slight, can be passed with assistance)
Average	930 ± 35	2214 ± 302	Success rate 40%
Mean velocity (mm/s)	0.43	0.18	-

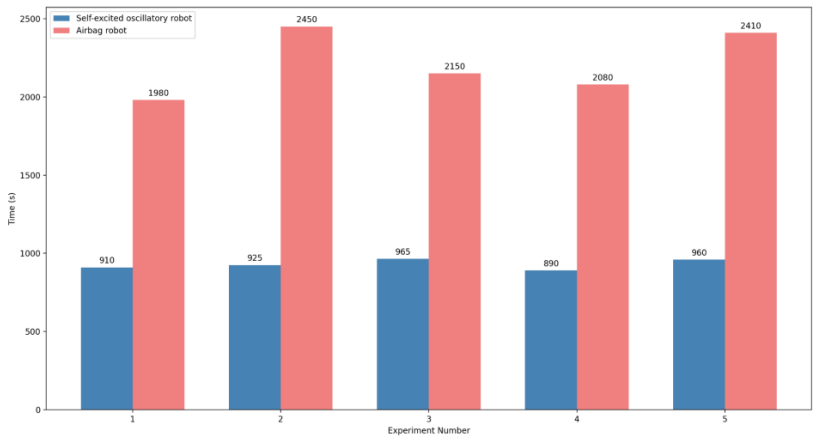


Figure 5-8: Comparison of transit time rates for a curved pipe (150° bend).

Experimental Results: Table 5-2 summarizes the data on the passage through curved pipes. Referring to Figure 5-8, the self-excited oscillation robot's average passage time across 5 experiments was 930 s, with a standard deviation of ±35 s, and an average arc speed of 0.43 mm/s, essentially the same as the straight pipe speed, indicating that active steering effectively compensated for the additional resistance caused by the curved path. All 5 experiments were completed on the first attempt without jamming, achieving a 100% success rate. The airbag robot's average passage time was 2214 s, with a standard deviation of ±302 s, and an average arc speed of 0.18 mm/s, which was lower than the straight-pipe speed. Only 2 out of 5 experiments resulted in successful passage through the curved pipe.

In contrast, 3 resulted in jamming (1 instance of complete jamming requiring manual intervention, and 2 instances of barely passing after assisted vibration), achieving a 40% success rate. The jamming was caused by the robot's inability to align with the curved pipe actively; alternating anchoring of the front and rear airbags created an imbalance in lateral forces, pushing the main body against the pipe wall. This experiment demonstrates the advantage of active steering when the robot moves through curved confined passages.

5.4 Adaptability Experiment in a Simulated Rubble Environment

To further evaluate the robot's applicability to post-disaster confined spaces, a simulated rubble environment was constructed using irregular blocks and debris. Unlike the standardized acrylic pipes used in the previous experiments, this environment contained uneven surfaces, curved paths, and narrow gaps. Two experimental scenarios were designed: movement along a curved path and passage through a narrow space.

5.4.1 Curved-Path Locomotion in the Rubble Environment

In the first scenario, irregular blocks were arranged to form a curved passage. The robot was placed at the entrance and operated under the same pneumatic condition used in the previous experiments. During movement, the airflow supplied to the two oscillation units was adjusted using the throttle valves to control the robot's direction.

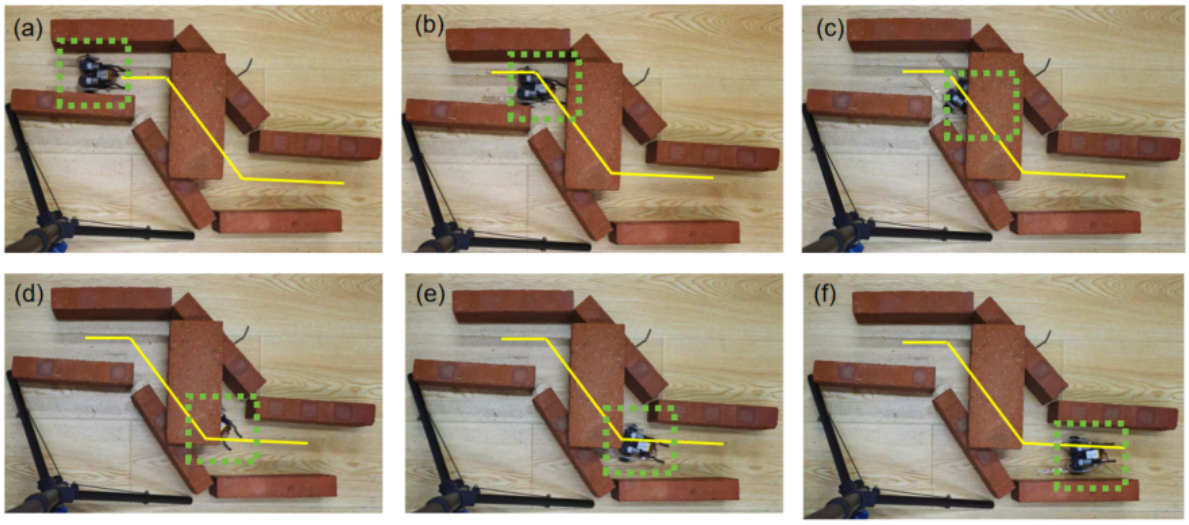


Figure 5-9: Sequential movement of the robot along a curved path in the simulated rubble environment: (a) initial position; (b) approaching the first bend; (c) entering the curved passage; (d) steering through the central bend; (e) exiting the curved passage; and (f) reaching the end of the path. The yellow line indicates the target path, and the green dashed box indicates the robot's position.

As shown in Figure 5-9, the robot moved through the curved passage by adjusting the airflow supplied to the two oscillation units. The sequence from (a) to (f) shows that the robot progressively changed its direction, passed around the irregularly arranged blocks, and reached the end of the path. This experiment demonstrates that the differential steering mechanism can operate in a simulated rubble environment.

5.4.2 Passage Through a Narrow Rubble Gap

In the second scenario, irregular blocks were arranged to form a narrow gap. The robot was placed in front of the gap and driven forward using the self-excited oscillation mechanism. During passage, the flexible oscillation units contacted the surrounding surfaces and underwent passive deformation.

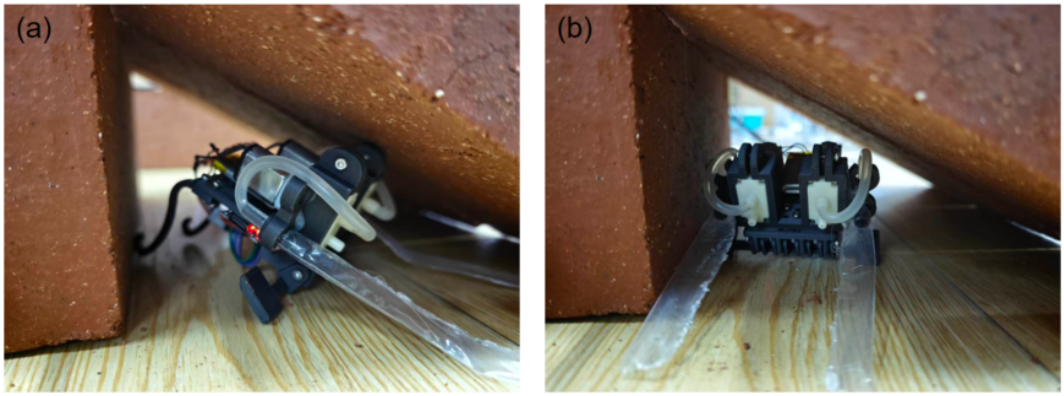


Figure 5-10: Passage of the robot through a narrow gap in the simulated rubble environment: (a) posture adjustment during contact with the inclined block; and (b) frontal view of the robot moving through the constrained space.

As shown in Figure 5-10, the robot adjusted its posture when contacting the inclined block and continued moving through the narrow gap. The flexible TPU oscillation units and compact body enabled the robot to adapt to the constrained space. This experiment demonstrates the passive deformation and narrow-gap passage capability of the robot in a simulated rubble environment.

The two experiments extend the standardized pipe tests to a more irregular environment. The curved-path experiment demonstrates the steering capability of the robot among rubble, while the narrow-gap experiment demonstrates the passive deformation and passage capability of its soft structure. These results provide preliminary evidence that the proposed robot can move through irregular and restricted spaces relevant to post-disaster exploration. However, further quantitative tests are required under more complex rubble conditions.

5.5 Comprehensive Analysis

Based on the above comparative experiments, the following comprehensive analytical conclusions can be drawn:

1. Axial motion efficiency: The linear motion speed of the self-excited oscillation robot (0.42 mm/s) is 2.2 times that of the airbag robot (0.19 mm/s). This advantage stems from the high-frequency, continuous-propulsion mode of self-excited oscillation: each oscillation cycle (approximately 0.19 s) produces a small displacement that accumulates to produce smooth motion. In comparison, the airbag robot generates only one large displacement per peristaltic cycle (approximately 5–10 s), with a long inflation/deflation waiting time in between. From an energy utilization perspective, self-excited oscillation directly converts constant air pressure into continuous kinetic energy, thereby avoiding energy loss from frequent solenoid valve switching.

2. Steering capability: Active steering is the core innovation of the self-excited oscillation robot. Controllable deflection can be achieved with simple unilateral throttling at an angular velocity of 2.33°/s, demonstrating its ability to adjust direction in curved confined passages. The 100% success rate in the 150° bend experiment contrasts sharply with the 40% success rate of the airbag robot, highlighting the importance of active steering in curved and irregular confined passages. It is worth noting that the basic steering mechanism does not require electronically timed valve switching, which reflects the advantages of physical intelligence—the control signal is "encoded" in the fluid network.

3. Control complexity and reliability: The self-excited oscillation robot generates periodic motion without solenoid-valve timing control. Its pneumatic system uses two independent micro air pumps and two manual throttle valves, whereas the airbag robot requires six solenoid valves, a microcontroller, and supporting circuitry. This simplified structure reduces the number of control components and potential failure points.

4. Rubble-environment adaptability: The curved-path experiment demonstrated that differential airflow could be used to adjust the robot's direction among irregular blocks. The narrow-gap experiment showed that the TPU units could deform passively during contact with the surrounding surfaces. These results provide preliminary support for the use of the robot in post-disaster confined spaces.

5. Limitations and trade-offs: The steering response of the self-excited oscillating robot has a certain delay (it takes about 2–3 oscillation cycles from adjusting the throttle valve to the actual deflection), and the steering angular velocity is coupled with the forward speed (a decrease in flow on one side during steering will weaken the propulsion force on that side, which may affect the overall speed). In addition, the current design cannot achieve continuous steering in any direction (e.g., S-shaped curves that require multiple adjustments), which can be improved in the future by increasing the number of units or introducing a cascade layout.

5.6 Chapter Summary

This chapter verifies the significant advantages of self-excited oscillating soft robots in terms of axial motion speed, active steering capability, and simplified control through systematic comparative experiments:

- In a 300 mm straight pipe, the self-excited oscillation robot achieved an average speed of 0.42 mm/s, approximately 2.2 times that of the airbag robot (0.19 mm/s).
- In a 150° curved pipe, the self-excited oscillation robot achieved a 100% passage success rate, whereas the airbag robot achieved a success rate of 40%.
- The self-excited oscillation robot generated continuous motion and differential steering without requiring electronically timed solenoid-valve switching.
- The simulated rubble experiments demonstrated curved-path steering and narrow-gap passage, providing preliminary validation of the robot's adaptability to irregular confined spaces.

The experimental results demonstrate that the self-excited oscillation mechanism can provide continuous forward motion and differential steering with a simplified pneumatic control structure. The straight-passage, curved-passage, and simulated rubble experiments provide preliminary validation of the robot's potential for post-disaster confined-space exploration. The next chapter summarizes the main findings and discusses future improvements.

6 Conclusions and Outlook

6.1 Summary of Research Work

This study developed a self-excited oscillation soft robot for post-disaster confined-space exploration. Based on the Flat Ring Tube (FRT) principle, TPU oscillation units with different lengths and widths were fabricated and tested. A unit with a width of 10 mm and a length of 80 mm was selected for robot integration. At an airflow rate of 0.8 L/min, its oscillation frequency was approximately 5.2 Hz.

The completed robot used two symmetrically distributed oscillation units. Similar airflow on both sides generated forward motion, while differential airflow enabled steering. Experiments showed that the robot achieved an average forward speed of 0.418 mm/s and an average steering angular velocity of 2.33 degrees/s.

The robot successfully moved through standardized passages with diameters of 80–120 mm under both dry and wet conditions. In the comparative experiments, its average speed in a 300 mm straight pipe was 0.42 mm/s, approximately 2.2 times that of the airbag robot (0.19 mm/s). In a 150-degree curved pipe, the proposed robot achieved a 100% passage success rate, compared with 40% for the airbag robot.

Two additional experiments were conducted in a simulated rubble environment. The robot followed a curved path among irregular blocks and passed through a narrow gap by using differential steering and passive deformation. These results provide preliminary validation of the robot's adaptability to irregular post-disaster confined spaces.

6.2 Outlook

The current robot remains at the prototype stage. Future work will focus on improving movement speed, obstacle-crossing capability, and resistance to puncture and abrasion. Automatic airflow control should also be introduced to replace manual throttle adjustment.

Cameras, microphones, gas sensors, and environmental sensors could be integrated for remote inspection and life-detection tasks. Further experiments should be conducted in larger and more realistic rubble environments containing dust, water, slopes, loose debris, and unstable obstacles. With these improvements, the robot could become a compact platform for preliminary search and environmental inspection in post-disaster confined spaces.

Reference

[1] Associated Press. Search for earthquake survivors enters final hours in Turkey. *Associated Press*, 2023. https://apnews.com/

[2] Reuters. Mapping the South Asia earthquake. *Reuters*, 2025. https://www.reuters.com/

[3] Reuters. Major tunnel and underground rescue operations. *Reuters*, 2026. https://www.reuters.com/

[4] Jacoff, A. S., Messina, E. R., and Weiss, B. A. Intelligent Systems for Urban Search and Rescue: Challenges and Lessons Learned. *Proceedings of SPIE*, vol. 5071, pp. 322–333, 2003. https://doi.org/10.1117/12.502415

[5] National Institute of Standards and Technology (NIST).*Statement of Requirements for Urban Search and Rescue Robot Performance Standards.*NIST, 2005.https://www.nist.gov/system/files/documents/el/isd/ks/Prelim_Requirements_Report.pdf

[6] Surmann, H. et al."Lessons from robot-assisted disaster response deployments by the German Rescue Robotics Center task force." *Journal of Field Robotics*, 2024.https://doi.org/10.1002/rob.22275

[7] Chen, T., Rushworth, A., Jia, F. et al. A Review on Search and Rescue Robots in Complex Scenarios: Key Technologies of Simultaneous Localisation and Mapping. *J. Field Robot.* (2026). https://doi.org/10.1002/rob.70256

[8] Jadeja, R., Trivedi, T., Surve, J. Survivor detection approach for post earthquake search and rescue missions based on deep learning inspired algorithms. *Sci Rep* 14, 25047 (2024). https://doi.org/10.1038/s41598-024-75156-z

[9] Blewitt, G., Cheneler, D., Andrew, J., Monk, S. A review of worm-like pipe inspection robots: research, trends and challenges. *Soft Sci* 4, 13 (2024). https://doi.org/10.20517/ss.2023.49

[10] Michael H. Dickinson et al.,How Animals Move: An Integrative View.*Science*288,100-106(2000). DOI: https://doi.org/10.1126/science.288.5463.100

[11] Chen, G., Long, Y., Yao, S. et al. A non-electrical pneumatic hybrid oscillator for high-frequency multimodal robotic locomotion. *Nat Commun* 16, 1449 (2025). https://doi.org/10.1038/s41467-025-56704-1

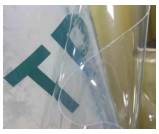
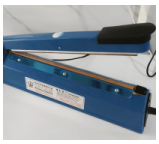
[12] Daniel J. Preston et al., A soft ring oscillator. *Sci. Robot.*4,eaaw5496(2019). DOI: https://doi.org/10.1126/scirobotics.aaw5496

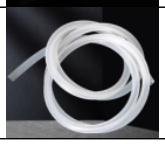
[13] H. Tsukagoshi, A. Kitagawa, K. Tambo, H. Chiba, A fluid self-excited oscillation peculiar to flat ring tube and its application to wearable robots, *Proceedings 2007 IEEE International Conference on Robotics and Automation* (2007), pp. 3138–3139.

[14] Niiyama R, Seong YA, Kawahara Y, Kuniyoshi Y. Blower-Powered Soft Inflatable Joints for Physical Human-Robot Interaction. *Front Robot AI.* 2021 Aug 24;8:720683. doi: https://doi.org/10.3389/frobt.2021.720683. PMID: 34504872; PMCID: PMC8421686.

[15] Nabae, H., Kitamura, E. (2022). Self-excited valve using a flat ring tube: Application to robotics. *Frontiers in Robotics and AI*, *9*, 1008559. https://doi.org/10.3389/frobot.2022.1008559

Appendix I

Name	Picture	Specifications	Functionality
Micro vacuum pump		Voltage: DC 5V Maximum inflation pressure: 60KPa Maximum vacuum pressure: -40KPa Maximum flow rate: 0.8L/min Weight: 15g	The pump provides a constant input to the robot's oscillation. It provides continuous pressure to inflate the film chamber, enabling bending and contraction. It serves as an anchor for the robot's self-oscillation and physical intelligence.
TPU film		Shore Hardness: 85A, 95A	TPU Film is the key material for the robot's pneumatic structure. The elasticity and durability provide a design with an appropriate thickness that enables gentle yet firm interactions.
ESP32 mini		Voltage: DC 5V	It helps regulate and quantify the pump's power. The ESP32 mini primarily affects the stability and frequency of the robot's oscillations.
Laminating machine		20*2mm	This is the fabrication tool I used to seal the TPU film layers with heat, generating bounded chambers with a consistent size for oscillation and sealing, ensuring stable pressure and exertion.
Air Pressure Sensor Module		Pressure detection range: 0-100Kpa	It serves as a measurement tool for the soft robot's self-oscillation, detecting its pressure and frequency behavior and quantifying its performance.
Switch		-	Repeatedly reduces the pump's power during testing.

Name	Picture	Specifications	Functionality
High-temperature resistant tape		-	The tape can be used to secure connecting joints and seams, thereby preventing loose ends and fittings that could adversely affect oscillating movement.
Hose connector		Converting a 3.2mm pipe diameter to a 6.4mm diameter pipe.	The two distinct hose connector sizes (4mm and 10mm in diameter) connect the hose to the pump.
Hose		Inner diameter 4mm	Transmission of gas from the pump.

Acknowledgments

I would like to express my sincere gratitude to everyone who contributed to completing this research project. Without their unwavering support and guidance, this work would not have been possible. My inspiration for this project came from an unexpected source: a 1999 Discovery Channel documentary called Insectia. One episode showed how insects move through rhythmic muscle cycles, the continuous interaction between the insect's musculoskeletal system and the external environment. It is a biological mechanism that allows motion to emerge through efficient, adaptable method without complex control systems. This single image sparked an idea within me, as I began exploring how that same principle could apply to a soft robot, encoding the control logic directly into the robot's physical design. Hence came to the system design that could navigate various damp, curved, narrow, and other irregularly structured areas with more flexibility, affordability, and convenience.

First of all, I am grateful to Mr. Tyler Ortiz for his guidance and suggestions on the technical feasibility during the project's progress. During the research period, we held regular monthly discussions to communicate about the current progress of the project, possible problems in the technical implementation, and the subsequent research directions. When I, as a high school researcher, encountered difficult problems that I could not confidently judge in areas such as mechanical structure, understanding of self-excited oscillation principles, experimental design, or technical implementation, Mr. Tyler Ortiz could provide suggestions from the perspective of engineering feasibility and research logic, helping me further clarify the problems and refine the research direction. These discussions enabled me to understand the complete process of "posing questions - verifying hypotheses - analyzing results - improving design" more systematically in the research process.

I would like to thank Dr. DelVecchio, my junior-year advisor in my school, for her ongoing support of the research process for this project and her insight comments during the drafting process and time management decisions to balance my academic and extracurricular work. She was the best advisor that I could ever ask for during the rigorous junior academic year.

I would also like to thank Ms. Grant for her tremendous support and helpful feedback in the biomimetic robot movement implementation, specifically regarding the study of musculoskeletal movement of the insects.

I acknowledge the foundational work of numerous international and well-established researchers and scholars cited in this paper, as their pioneering work provided indispensable context and references for this project.

I would like to give thanks to my school for help cultivating and facilitate my interest in biomedical engineering. It is no easy feat to help a boarding school student coordinate extracurricular activities outside of regular school calendars. The Thacher School's four fundamental pillars: Honor, Fairness, Kindness, and Truth foster resilient and noble scholarship with great versatility and the willingness to exceed expectations. Those core values are made evident throughout this research process, my academic journey as a scholar, and my personal life as an honorable young adult.

I acknowledge that I used ChatGPT Plus (GPT-5.6 Sol) for limited assistance with English grammar checking, language refinement, figure and chart presentation, and LaTeX formatting verification. I did not use AI for research question formulation, experimental design, prototype development, data analysis, result interpretation, or conclusion generation. All substantive research work was independently completed by me.

Last but definitely not the least, I would love to thank my lovely parents for their endless love and unwavering support throughout my journey.